Department of Chemistry and Materials Science

Role of potassium hydroxide in fouling and fireside corrosion processes in biomass-fired boilers

Tom Blomberg

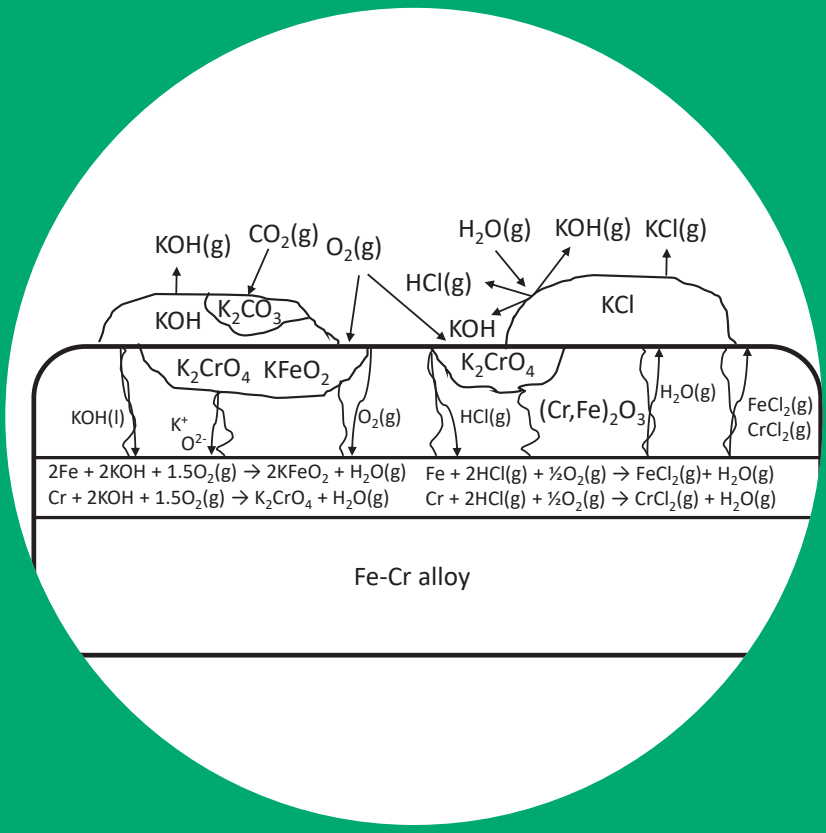

Aalto University

DOCTORAL DISSERTATIONS

Aalto University publication series
DOCTORAL DISSERTATIONS 35/2020

Role of potassium hydroxide in fouling and fireside corrosion processes in biomass-fired boilers

Tom Blomberg

M.Sc.(Tech.) Tom Blomberg will defend the dissertation "Role of Potassium Hydroxide in Fouling and Fireside Corrosion Processes in Biomass Fired Boilers" on 14 August 2020 at 12 in Aalto University School of Chemical Engineering, Department of Chemistry and Materials Science.

Aalto University
School of Chemical Engineering
Department of Chemistry and Materials Science

Supervising professor
Professor Maarit Karppinen, Aalto University, Finland

Thesis advisor
Professor Maarit Karppinen, Aalto University, Finland

Preliminary examiners
Professor Nigel Simms, Cranfield University, United Kingdom
Associate Professor Flemming Frandsen, Technical University of Denmark, Denmark

Opponent
Professor Mikko Hupa, Åbo Akademi, Finland

Aalto University publication series
DOCTORAL DISSERTATIONS 35/2020

ISBN 978-952-60-8982-9 (printed)
ISBN 978-952-60-8983-6 (pdf)
ISSN 1799-4934 (printed)
ISSN 1799-4942 (pdf)
http://urn.fi/URN:ISBN:978-952-60-8983-6

Unigrafia Oy
Helsinki 2020

Finland

Printed matter
4041-0619

Aalto University

Abstract

Aalto University, P.O. Box 11000, FI-00076 Aalto www.aalto.fi

Author
Tom Blomberg

Name of the doctoral dissertation
Role of potassium hydroxide in fouling and fireside corrosion processes in biomass-fired boilers

Publisher School of Chemical Engineering

Unit Department of Chemistry and Materials Science

Series Aalto University publication series DOCTORAL DISSERTATIONS 35/2020

Field of research Inorganic Chemistry

Manuscript submitted 12 November 2019 **Date of the defence** 20 March 2020

Permission for public defence granted (date) 12 February 2020 **Language** English

☐ **Monograph** ☒ **Article dissertation** ☐ **Essay dissertation**

Abstract

Slagging, fouling and fireside corrosion in biomass fuelled boilers and gasifiers are major obstacles that diminish the efficiencies of the energy transformation processes in these systems. High chemical to thermal and thermal to electric conversion efficiencies require high surface temperatures in the equipment construction components. This leads to increased risks of shortening the service life times of the components, when biomass based fuels are used in place of fossil fuels. The inorganic part of biomass fuels are different from fossil fuels and therefore lead to different ash behaviour in the combustors. Sulphur contents in fossil fuels are typically much larger than in biomass fuels, whereas the potassium contents in bio-mass based fuels are typically larger than in fossil fuels. During combustion, potassium is initially released in the gas phase as elemental potassium, potassium hydroxide or potassium chloride. These compounds then react with SiO_2(s,l,g), SO_2(g)/SO_3(g), HCl(g), and CO(g)/CO_2(g) in the combustor and play a major role in the slagging, fouling and corrosion processes. Most of the published scientific work done so far to understand these processes conclude that KCl(s,l,g) is the most important potassium compound responsible for the slagging, fouling and corrosion problems. The importance of KOH(s,l,g) in these processes has gained a lot less attention. In this thesis, the possible effect of KOH(s,l,g) in the fouling and corrosion issues was studied. Categorizing biomass and fossil fuels based on the free potassium content (potassium not bound as chloride or sulphate) was found to separate the biomass based fuels from fossil fuels. Biomass has typically free potassium, whereas fossil fuels do not. This difference suggests that during combustion and gasification, the potassium in the gas phase may exist as KOH(g) in the flue gases near the heat transfer surfaces. In addition, a correlation of KOH(g) with the corrosion rates of different steels in a straw fired boilers was found. Furthermore, using in-situ electrochemical galvanic probe measurements in a full-scale biomass fired boiler showed that the electrochemical signal activity increases abruptly at ≈ 400 °C. This may indicate the melting temperature of the condensing layer, which is very close to the melting point of KOH (406 °C), suggesting that condensation of KOH(l) can happen before reaction with CO_2(g) to form K_2CO_3(s). Finally, using laboratory exposures of KOH(s,l) and KCl(s,l) with Cr_2O_3(s) and Fe_2O_3(s) it was found out that the formation of K_2CrO_4(s) could be explained for both salts with similar mechanism: $4KOH(s,l) + Cr_2O_3(s) + 1½O_2(g) \rightarrow 2K_2CrO_4(s) + 2H_2O(g)$. This result sheds light on the initial breakdown mechanism of the protective oxides on high temperature steels in biomass combustion and gasification atmospheres. Overall, the conclusion is that KOH(s,l,g) may be a major reaction intermediate taking part in the slagging, fouling and corrosion mechanisms in biomass fired combustors.

Keywords biomass combustion, fouling, corrosion, potassium hydroxide, CO2 emission

ISBN (printed) 978-952-60-8982-9 **ISBN (pdf)** 978-952-60-8983-6

ISSN (printed) 1799-4934 **ISSN (pdf)** 1799-4942

Location of publisher Helsinki **Location of printing** Helsinki **Year** 2020

Pages 108 **urn** http://urn.fi/URN:ISBN:978-952-60-8983-6

Tekijä
Tom Blomberg

Väitöskirjan nimi
Kaliumhydroxidin rooli likaantumis– ja korroosioprosesseissa biomassaa polttavissa kattiloissa

Julkaisija Kemian tekniikan korkeakoulu

Yksikkö Kemian ja materiaalitieteen laitos

Sarja Aalto University publication series DOCTORAL DISSERTATIONS 35/2020

Tutkimusala Epäorgaaninen kemia

Käsikirjoituksen pvm 12.11.2019 **Väitöspäivä** 20.03.2020

Väittelyluvan myöntämispäivä 12.02.2020 **Kieli** Englanti

☐ **Monografia** ☒ **Artikkeliväitöskirja** ☐ **Esseeväitöskirja**

Tiivistelmä

Kuonaantuminen, likaantuminen ja korkean lämpötilan korroosio biomassaa käyttävissä kattiloissa ja kaasuttimissa ovat merkittäviä esteitä, jotka vähentävät energianmuutosprosessien tehokkuutta näissä järjestelmissä. Korkeat energian muuntohyötysuhteet vaativat korkeita pintalämpötiloja laitteistojen rakennekomponenteissa. Tämä lisää riskiä komponenttien käyttöiän lyhenemiseen, kun fossiilisten polttoaineiden sijasta käytetään biomassapohjaisia polttoaineita. Biomassapolttoaineiden epäorgaaninen osa eroaa fossiilisista polttoaineista ja johtaa siten erilaiseen tuhkan käyttäytymiseen tulipesässä ja savukaasukanavassa. Fossiilisten polttoaineiden rikkipitoisuudet ovat tyypillisesti huomattavasti suurempia kuin biomassapolttoaineiden, kun taas biomassapohjaisten polttoaineiden kaliumpitoisuus on tyypillisesti suurempi kuin fossiilisten polttoaineiden. Palamisen aikana kalium vapautuu kaasufaasiin alkuainekaliumina, kaliumhydroksidina tai kaliumkloridina. Nämä yhdisteet reagoivat sitten polttoaineen sisältämän SiO_2(s,l,g):n, SO_2(g)/SO_3 (g):n, HCl(g):n ja CO(g)/CO_2(g):n kanssa ja ovat tärkeässä roolissa tulipuolen kuonaantumis-, likaantumis- ja korroosioprosesseissa. Suurin osa tähän mennesssä tehdystä tieteellisestä työstä on käsitellyt KCl:n merkitystä edellä mainituissa prosesseissa. On päätelty, että KCl(s,l,g) on tärkein kaliumyhdiste, joka aiheuttaa kuonan muodostumista, likaantumista ja korroosiota. KOH(s,l,g):n merkitystä näissä prosesseissa on tutkittu paljon vähemmän. Tässä opinnäytetyössä tutkittiin KOH(s,l,g):n mahdollista vaikutusta likaantumis- ja korroosiprosesseihin. Biomassan ja fossiilisten polttoaineiden luokittelu vapaan kaliumpitoisuuden perusteella erotti biomassapohjaiset polttoaineet fossiilisista polttoaineista. Biomassa sisältää tyypillisesti vapaata kaliumia, kun taas fossiiliset polttoaineet eivät. Ero viittaa siihen, että polttoaineen palamisen ja kaasuuntumisen aikana kaasufaasissa oleva kalium voi esiintyä KOH(g):na savukaasuissa lähellä lämmönsiirtopintoja. Lisäksi löydettiin korrelaatio termodynaamisesti lasketun KOH(g):n suhteellisen osapaineen ja eri terästen korroosionopeuksien välille olkikattilassa. In-situ mittaukset sähkökemiallisella galvaanisella sondilla täysimittaisessa biomassaa polttavassa kattilassa osoittivat, että sähkökemiallisen signaalin aktiivisuus kasvaa äkillisesti lämpötilassa ≈ 400 ° C. Tämä saattaa viitata kondenssikerroksen sulamislämpötilaan, joka on hyvin lähellä KOH:n sulamispistettä (406 °C), mikä taas viittaa siihen, että KOH(l):n kondensoituminen voi tapahtua ennen reaktiota CO_2(g):n kanssa (muodostaen K_2CO_3(s):a). Laboratorioaltistustestit KOH(s, l):n, KCl(s,l):n ja Cr_2O_3(s):n sekä Fe_2O_3(s):n kanssa osoittivat, että K_2CrO_4(s):n muodostuminen voitiin selittää molemmille suoloille samanlaisella mekanismilla: $4KOH(s,l) + Cr_2O_3(s) + 1½O_2(g) \rightarrow 2K_2CrO_4(s) + 2H_2O(g)$. Tulos antaa lisätietoa korkeiden lämpötilojen terästen suojaavien oksidien hajoamismekanismista biomassaa käyttävissä poltto- ja kaasutusreaktoreissa. Loppupäätelmä on, että KOH(s,l,g) voi olla tärkeä reaktiovälituote, joka osallistuu biomassaa käyttävien polttoprosessien likaantumis- ja korroosiomekanismeihin.

Avainsanat biomassan poltto, likaantuminen, korroosio, kaliumhydroxidi, CO2 päästöt

ISBN (painettu) 978-952-60-8982-9 **ISBN (pdf)** 978-952-60-8983-6

ISSN (painettu) 1799-4934 **ISSN (pdf)** 1799-4942

Julkaisupaikka Helsinki **Painopaikka** Helsinki **Vuosi** 2020

Sivumäärä 108 **urn** http://urn.fi/URN:ISBN:978-952-60-8983-6

Preface

The foundations of this work were laid down in 1999 when I was working as a research engineer at the R&D centre of Foster Wheeler Energia Oy in Karhula, Finland. Foster Wheeler Corporation had bought the circulating fluidized bed (CFB) boiler business from Ahlstrom Oy in 1995. By the mid-late 1990s, there was a substantial effort to expand the CFB combustion technology to other fuels than coal. At the time, the fouling and corrosion issues in the boilers when using biomass-based fuels instead of coal became apparent, and my project was to develop a method that could be used to monitor fireside corrosion in the boilers. During the year 1999, the development led to the electrochemical on-line corrosion probe using the galvanic couple principle (Publication I and (Blomberg, Hiltunen, & Makkonen, 2001)). The probe is still commercially available from Coresto Oy, but with more sophisticated electrochemical measurements (LPR) added (Tuurna, 2011; Mahanen, Vänskä, & Zabetta, 2015). The galvanic probe was tested in the pilot plant CFB facility in Karhula and in the autumn of 1999, it was also tested in full-scale tests in the Högdalen CFB boiler in Stockholm, Sweden (Publications I and Blomberg, Hiltunen, & Makkonen, 2001). It was discovered with the electrochemical probe measurements that the galvanic voltage and currents started to show electrochemical activity around 400 °C metal surface temperature in boilers combusting virgin biomass (wood, straw etc.), whereas with waste biomass the electrochemical activity started at temperatures as low as approximately 200-250 °C metal surface temperatures. The simplest interpretation of the sudden increase in the galvanic couple signals as a function of temperature was that a molten phase was formed at this temperature on the metal surface and the ionic conduction of the melt completed the galvanic couple circuit. This assumption is of course not very scientific, because there is a possibility that solid phases at these material temperatures may also become ionically conductive. Nevertheless, the assumption that we were measuring the melting point of the deposit on-line led us to the search for a compound that could explain this melting temperature around 400 °C. Earlier studies had indicated the melting behaviour of alkali salt mixtures of sulphates, chlorides and carbonates to be around 500 °C at the lowest, and our on-line measured melting point was 100 °C lower than this value. Furthermore, with short exposure time measurements conducted in the combustion tests in the pilot facility using straw gasification fly ash as fuel, we could see that the galvanic couple signal jumped immediately (in seconds) when starting the straw gasification fly ash feed into the boiler that was already operating at high temperatures with natural gas combustion. This observation suggested that the melt is formed immediately on the probe surface when the biomass is combusted and does not require an incubation period in the beginning of the deposit formation process, as would have been expected in case the melt formation, which would have required first gas–solid or solid–solid corrosion reactions between the deposit and metal to take place. Quite quickly, it became clear that if KOH(l) were to be the condensing substance on the tube surface, it would neatly explain our experimental findings with the galvanic probe.

The next task was to show how KOH(g) could still survive in the flue gases and not react to KCl(s,l,g), K_2SO_4(s,l,g) or K_2CO_3(s,l) in the flue gases before reaching the tube surface. This led to the calculation of the free alkali index (Publications I and II and Blomberg, 2007). The index is based on simple molar balance calculations of K, Na, S and Cl in the fuel. Fortunately, in the fuel laboratory of Karhula R&D centre, these analyses had been done for a number of fuels already (only the S content in the fuel is part of the standard ultimate analysis, and therefore, the K, Na and Cl contents in the fuel are not part of standard fuel analysis and having these values for the fuels was not obvious). When sorting the fuels with the aid of this parameter, it became apparent that biomass-based fuels had positive indices and fossil fuels had negative indices. This was amazing, as it seemed that this very simple fuel index could categorize biomass fuels and fossil fuels into two separate groups from the point of view of deposit formation.

I resigned from Foster Wheeler Energia Oy in 2000, but this difference between biomass-based fuels and fossil fuels kept haunting my thoughts. By 2009, I had built a more complete chemical model on the behaviour of potassium in biomass-fired boilers and published my ideas in a Dechema workshop, 'High Temperature Corrosion Protection in Energy Conversion Systems', in 2009 at Frankfurt am Main (Publication III). In 2011, I found a correlation between the calculated amount of KOH(g) in the flue gases and the measured corrosion rates in a straw-fired boiler (Publication IV). At this time, I thought I had enough indirect evidence that KOH(g) → KOH(s,l) condensation must indeed play a role in the fouling and corrosion reactions in biomass combustions (as we already thought in late 1990s), but needed more experimental proof. So, after 20 years working in industry, I returned to academia to study the problem with laboratory tests. This led to the latest publication included in this thesis (Publication V). In this publication, it is shown that you can in fact explain the corrosion reactions of KCl with the protective oxides of the superheater tubes in water-containing high temperature environments simply by assuming that it first decomposes into KOH(s,l) and HCl(g) and then the formed KOH(s,l) will react with the protective oxide. This finding provides a possibility for further unification of the corrosion mechanisms in biomass-fired boilers with KCl(s,l) or KOH/K_2CO_3(s,l) as the corroding substances.

I am grateful to my Professor, Maarit Karppinen, who has supported me throughout the finalization of the work. She possesses not only enormous intelligence, but also a great deal of wisdom, and still she remains humble and always willing to help. I also want to thank the Academy of Finland and the Finnish Environment Institute for financing the work related to the latest publication in this thesis (Publication V) through the CloseLoop project. I would also like to mention how grateful I am for the Finnish educational system, which enables a high education level for people regardless of their financial means and family background. Thank you to my mother and family for providing me a secure and happy childhood. Finally, I want to thank my spouse, Riia, for all the support, understanding and love I have received and continue to receive. I dedicate this thesis to my brother and father who passed away too early from this life.

Tom Blomberg

“For a successful technology, reality must take precedence over public relations, for Nature cannot be fooled”

-Richard Feynman

Role of potassium hydroxide in fouling and fireside corrosion processes in biomass-fired boilers

Table of contents

List of publications

Journal articles:

I. Blomberg, T., Makkonen, P., Hiltunen, M., Role of Alkali Hydroxides in the Fireside Corrosion of Heat Transfer Surfaces, a Practical Approach, **Materials Science Forum**, Vol. 461-464, (2004), pp.883-890.

II. Blomberg, T., Which are the right test conditions for the simulation of high temperature alkali corrosion in biomass combustion? **Materials and Corrosion**, 57, (2006), pp.170-175.

III. Blomberg, T., A thermodynamic study of the gaseous potassium chemistry in the convection sections of biomass fired boilers, **Materials and Corrosion**, 62, (2011), pp.635-641.

IV. Blomberg, T., Correlation of the corrosion rates of steels in a straw fired boiler with the thermodynamically predicted trend of KOH(g) in the flue gases, **Biomass and Bioenergy**, 39, (2012), pp.489-493.

V. Blomberg T., Tripathi, T., Karppinen, M., New chemical mechanism explaining the breakdown of protective oxides on high temperature steels in biomass combustion and gasification plants, **RSC Advances,** 9, (2019), pp.10034-10048.

Author's contribution

I. The author developed and built the galvanic probe, conducted the measurements, processed the data and wrote the publication, apart from the introduction section. Pasi Makkonen wrote the introduction section. Pasi Makkonen and Matti Hiltunen helped in the writing of the paper and gave guidance during the course of the work.

II. The author was the only contributor to the article.

III. The author was the only contributor to the article.

IV. The author was the only contributor to the article.

V. The author planned the work, conducted the measurements, processed the data and wrote the publication. Tripathi Tripurari helped in the writing of the paper. Maarit Karppinen suggested some changes in the way of presenting the data, which were included. Both Tripathi Tripurari and Maarit Karppinen provided guidance during the course of the work.

List of abbreviations and symbols

A	absorbance
$[K_{sol}]$	acetic acid soluble fraction of the potassium in the fuel, mol/kg fuel
$[Na_{sol}]$	acetic acid soluble fraction of the sodium in the fuel, mol/kg fuel
a_j	activity coefficient of individual component in the products of reaction
a_i	activity coefficient of individual component in the reactants of reaction
(ads.)	adsorbed phase
(aq)	aqueous solution
BCC	body-centred cubic
k	Boltzmann's constant
BFB	bubbling fluidized bed
E_{cell}^0	cell potential in standard conditions
q	charge
μ_i	chemical potential of pure compound
[Cl]	chlorine content of the fuel, mol/kg fuel, dry basis
CFB	circulating fluidized bed
CFD	computational fluid dynamics
c	concentration of the molecule in the sample
x	conversion of fuel alkali to vaporized alkali
η	dynamic viscosity of the fluid
EIS	electrochemical impedance spectroscopy
EN	electrochemical noise
FCC	face-centred cubic
F	Faraday's constant
R	gas constant

(g)	gas phase
ΔG_f	Gibbs free energy change of a reaction
ΔG_{mix}	Gibbs free energy change when forming a mixture
ΔC_p	heat capacity change in a reaction
$\dot{Q}$	heat flow
HHV	higher heating value
θ	incident angle of the X-rays
n	integer
I	intensity of the light beam with the sample
I_0	intensity of the light beam without the sample
LPR	linear polarization resistance
(l)	liquid phase
LHV	lower heating value
D_m	mass diffusion coefficient
$\dot{W}$	mechanical work flow = power
ε	molar absorptivity of the molecule
$\frac{dn}{dt}$	molar flow rate of ions
n_i	mole number of the component
NTP	normal temperature and pressure
N	number of components
z	number of electrons transferred in the cell reaction
ORC	organic Rankine cycle
p_i	partial pressure of the component
d	particle diameter
ppm(v)	parts per million in volume

[K]	potassium content of the fuel, mol/kg fuel, dry basis
p	pressure
PF	pulverized fuel
S	saturation ratio
$p_i(sat)$	saturation vapor pressure of the component
[Na]	sodium content of the fuel, mol/kg fuel, dry basis
(s)	solid phase
S_T	Soret coefficient
d	spacing between the lattice planes
ΔH_f^0	standard enthalpy of formation
ΔS_f^0	standard entropy of formation
ΔG_f^0	standard Gibbs free energy of formation
ν_j	stoichiometric coefficient of the individual component in the products of reaction
ν_i	stoichiometric coefficient of the individual component in the reactants of reaction
[S]	sulphur content of the fuel, mol/kg fuel, dry basis
T	temperature
D_T	thermal diffusion coefficient
b	thickness of the sample
G_f^{total}	total Gibbs free energy of the system
UV	ultra-violet
λ	wavelength
w-%	weight percent
VIS	visible
XRD	x-ray diffraction

1. Research objectives

This thesis deals with fouling and high temperature corrosion in furnaces and boilers using biomass-based fuels as their energy source. The inorganic composition of biomass-based fuels differs from coal and leads to increased fouling and corrosion rates in the combustors. This has forced the biomass-fired combustors to operate at lower heat transfer surface temperatures, which leads to efficiency penalties compared to fossil fuel fired units. In addition, unscheduled maintenance breaks and corrosion of the construction materials increases the operation costs. Ash behaviour in the combustor, especially the behaviour of alkali metals, chlorine and sulphur, has been identified as the key to understanding and mitigating fouling and corrosion issues in the combustors. Understanding the process chemistry of these elements in the combustors may lead to new methods of mitigating these issues and enable the biomass-fired units to operate at higher conversion efficiencies. Potassium is the major alkali in biomass based fuels, and substantial scientific work has already been done to understand its behaviour in the combustors. The earlier work has mostly concentrated on the fate of potassium chloride (KCl), because this compound is frequently found on heavily fouled and corroded heat transfer surfaces. This thesis is concentrated on the effect of potassium hydroxide (KOH) as a possible fouling/corrosion agent and as a possible precursor for KCl formation. The research questions that this thesis tries to address are as follows:

1. Is it possible that KOH(s,l,g) is present in the flue gases in the superheater area when biomass based fuels are fired?
2. If present in the flue gases, can KOH(g) condense as KOH(s,l) on the heat transfer surfaces, or is all released KOH(g) consumed in reactions to K_2SO_4(s,l,g), KCl(s,l,g) and K_2CO_3(s,l,g) before reaching the heat transfer surfaces?
3. What should the laboratory test environment be in order to adequately simulate the corrosion environment in real combustors?
4. What could the chemical mechanism be of steel corrosion in biomass-fired units if KOH(s,l,g) plays an active role in the corrosion reactions?

Obviously, the research problem is extremely complex, as the ash chemistry in combustion can be very complicated. When a large amount of biomass is combusted, then even trace amounts in the ash-forming elements can accumulate in the boiler, causing fouling and corrosion. It is difficult to say with certainty that one mechanism is more pronounced than the other. However, in engineering analysis, one tries to find the most influential mechanism, not necessarily all the possible mechanisms affecting the issue. Therefore, we suggest hypotheses and test those hypotheses with experiments and models.

2. Heat and electricity generation and global CO_2 emissions

The mitigation of human-induced global warming is one of the greatest challenges mankind is facing. The industrialization period responsible for human-induced global warming is approximately 200 years in length. In geological time scales, this is an extremely short period of time. However, human activity on earth has resulted in an unprecedented increase in the emissions of greenhouse gases. This may lead to the increase of the average temperature of the globe and induce climate change that risks the lives of millions, if not billions of people in the future. Although not

the most severe greenhouse gas, CO_2 emissions are one of the most difficult to mitigate. CO_2 is produced as a by-product from combustion processes that provide the major share of the energy production, driving our technical development and economic growth. Figure 1 presents the global CO_2 emissions by sector. Heat and electricity production accounts for 42% of all the CO_2 emissions. Burning coal to produce electricity accounts for about 41% of the total electricity generation, and therefore global CO_2 emissions from coal use in electricity generation alone account approximately 16% of the total. Adding the industrial use of coal (mainly in the steel industry) results in a figure of 25% of the total anthropogenic CO_2 emissions from the use of coal. In absolute terms, this is about 9 Gtons of CO_2 emissions per year (IEA, 2017). Biomass is considered CO_2 neutral, because the CO_2 emissions released during combustion are absorbed back into the biomass during its growth cycle. When replacing coal with sustainable biomass, the net CO_2 emission can be reduced compared to coal. However, the sustainability criteria of biomass used as fuel needs careful consideration.

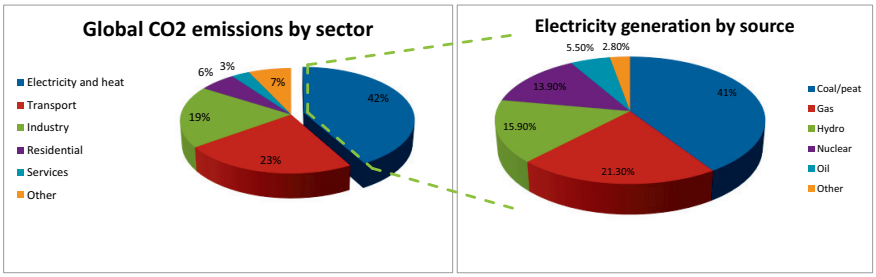

Figure 1. Global CO_2 emissions by sector and electricity generation by source (IEA, 2017) .

The cultivation of energy crops for fuel usage may compete with land usage for food production. Furthermore, a sudden increase in the usage of forest-based biomass as fuels leads to a short-term net increase in CO_2 emissions for many decades, due to their long carbon cycle lengths. There is also a risk that the cut forests do not necessarily regenerate as they were, due to erosion effects after the protecting forest cover has been removed. This may decrease the total carbon stock available in forests. Therefore, short carbon cycle fuels, such as surplus agricultural residues, should be preferred in energy production (Liu, et al., 2017). Unfortunately, these fuels are technologically more difficult to combust due to their lower volume density, higher ash, alkali (K, Na) and chlorine contents compared to wood.

2.1 Rankine cycle

Practically all electricity generation using solid fuels is done by the Rankine cycle. Some power plants use solid fuel gasification to provide gaseous fuel for a combustion turbine (Brayton cycle), but the number of these plants is marginal and can be considered proof of concept pilots rather than significant technology for electricity generation at present. Figure 2 presents a schematic of the Rankine cycle. The benefit of the Rankine cycle is its simplicity, robustness and still high heat to work efficiently. In the Rankine cycle, the combustion environment is decoupled from the turbine environment, and therefore it is suitable for many types of fuels. The fuel provides the heat energy that is transferred to the working fluid with the aid of heat exchangers installed in the boiler. Ordinary water is used as the working

fluid in the original Rankine cycle, but for low temperature application, organic working fluids with lower boiling points have also been used. These are called organic Rankine cycle (ORC) systems. The thermal efficiency of the Rankine cycle depends on the thermodynamic properties of the working fluid. High pressure and temperature at the inlet of the steam turbine, and low pressure and temperature at the condenser, increase the thermal efficiency.

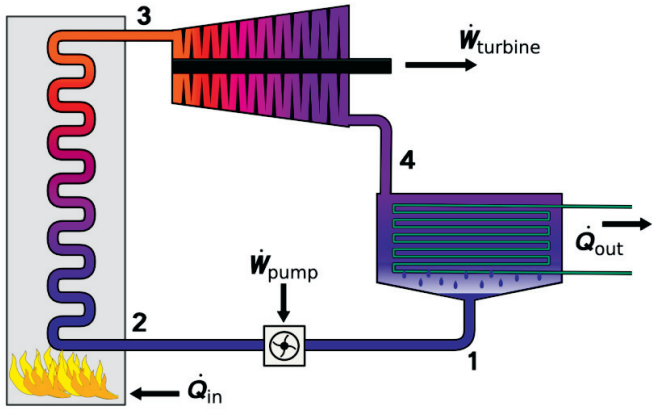

Figure 2. Schematic presentation of the Rankine cycle. Reproduced from Andrew.Ainsworth at English Wikipedia, under CC BY-SA 3.0 license.

The electrical efficiency also depends on many other factors, such as the heat to work efficiency of the steam turbine and the work to electricity efficiency of the generator. However, from the boiler design point of view, the electrical efficiency can be increased by increasing the temperature and pressure of the steam circuit. This increases the material surface temperatures in the heat exchangers, which typically leads to a higher corrosion rate of the alloys used to construct them. The corrosion rate of the materials limits the maximum temperature of the heat exchangers and therefore also the thermodynamic efficiency of the cycle. The best electrical efficiencies achieved in practice for the Rankine cycle using coal as fuel are in the 45-47% (LHV) range (Santoianni, Dawn, 2015), but when using biomass as the only fuel, the best efficiencies achieved are normally in the 30-35% (LHV) range (van den Broek, FaaiJ, & van Wijk, 1996). Part of this efficiency gap can be explained by the typically smaller unit sizes of biomass-burning boilers, because of the local nature of biomass fuel production, but a major issue is also the higher fireside corrosion rate of the heat exchanger materials when using biomass fuels instead of coal.

Co-firing biomass either directly (mixed in the furnace with coal) or indirectly (combusted in a separate boiler with low steam temperatures and combining the steam flows) with coal results in lower corrosion rates than pure biomass firing. In the former case, the lower corrosion rate is due to the interactions of the coal sulphur and ash minerals, gettering some of the alkali released from the biomass and leading to a less corrosive environment in the boiler. In the latter case, the lower corrosion rates are achieved by lowering the surface temperatures of the heat exchangers in the biomass-only burning unit, and then doing the final superheating of the steam flow with the coal firing unit. With direct co-firing, electrical efficiencies are typically in between the biomass-only and coal-only units, because of the still higher corrosion rates than in the coal only units. However, ash

disposal is problematic with direct co-firing. Coal ash has been used as an ingredient in the brick and concrete industry, but the altered ash composition as a result of co-firing with biomass may prevent its usage in these applications. On the other hand, ash from biomass-only firing units can normally be used as a fertilizing agent because it contains a large amount of water-soluble potassium compounds (plant nutrient) and very low amounts of heavy metals. Therefore, from the ash disposal point of view, indirect co-firing is more convenient, but the technology is more expensive and complicated because it requires two separate boiler units in the power plant (Karampinis, Grammelis, Agraniotis, Violidakis, & Kakaras, 2014).

2.2 Mass and energy balance of a boiler

Boilers are energy conversion devices that convert the chemical energy stored in the chemical bonds of the fuel to the heat energy of water and steam. The energy released in the combustion of solid fuel depends on the organic compounds it consists of. The detailed chemical identification of all the chemical compounds a fuel contains is not possible in practice. Therefore, for practical reasons, the heating value of the fuel is either measured in a bomb calorimeter by combusting a sample of the fuel in pure oxygen and measuring the heat released, or by estimating it from the elemental analysis of the fuel. The elemental analysis of the major elements (C, H, O, N, S) contained in the fuel is called the ultimate analysis in fuel science. Using the ultimate analysis, a fairly accurate estimation of the heating value can be made with empirical correlations (Demirbas & Ayhan, 1997; Channiwala & Parikh, 2002). There are two heating values that are frequently used: lower heating value (LHV) and higher heating value (HHV). The difference between them is the reference temperature of the water in the flue gases after complete combustion of the fuel. In LHV, the reference temperature is 100 °C, and in HHV, it is 25 °C. LHV better presents the maximum energy that can be extracted from the fuel in practice, because the temperature of the flue gases at the outlet of the chimney has to be kept higher than 100 °C to prevent condensation of water in the flue gas duct. If water is let to condense in the flue gases, it reacts with SO_3(g) and HCl(g) present in the flue gases, forming sulphuric or hydrochloric acid – or a mixture of them – that corrodes the low temperature section of the boiler (acid dew point corrosion) (Herzog, et al., 2012). Only in cases where the boiler is equipped with wet flue gas scrubber or is designed for condensing operation can the remaining heat energy be extracted (Neuenschwander & Good J, 1998). When comparing the electrical efficiency values reported for plants, it is important to know to which heating value the efficiency calculation refers in order to make a fair comparison.

Figure 3 shows schematic figures of different types of boilers. Mass flow of fuel is fed to the furnace section of the boiler, where its chemical energy is transformed to heat energy in the combustion process. The maximum theoretical combustion efficiency is achieved with stoichiometric combustion. If the oxygen content is lower than the stoichiometric oxygen content, then it leads to efficiency penalties due to the unburned carbon content in the flue gases (C_xH_y(g) and CO(g) plus organic C in fly ash). If the oxygen content is higher than the stoichiometric oxygen content, then it leads to thermal efficiency penalties due to dilution of the flue gases with non-reacting gases (N_2, excess O_2). So in theory, the goal of the furnace design is to provide a perfect mixing of the fuel with the stoichiometric amount of combustion air and sufficient residence time for the combustion reactions to reach thermodynamic equilibrium before escaping the furnace. In practice, this is impossible, and therefore practical units operate with certain amounts of excess

oxygen at the furnace outlet in order to reach high combustion efficiencies. Typical combustion efficiencies in modern, large-scale circulating fluidized bed (CFB) boilers firing reactive fuels such as lignite or biomass are 99-100% (boiler efficiencies > 90% (LHV)), achieved with 3-4 vol-% oxygen in the flue gases at the furnace outlet (Jeng, et al., 2009).

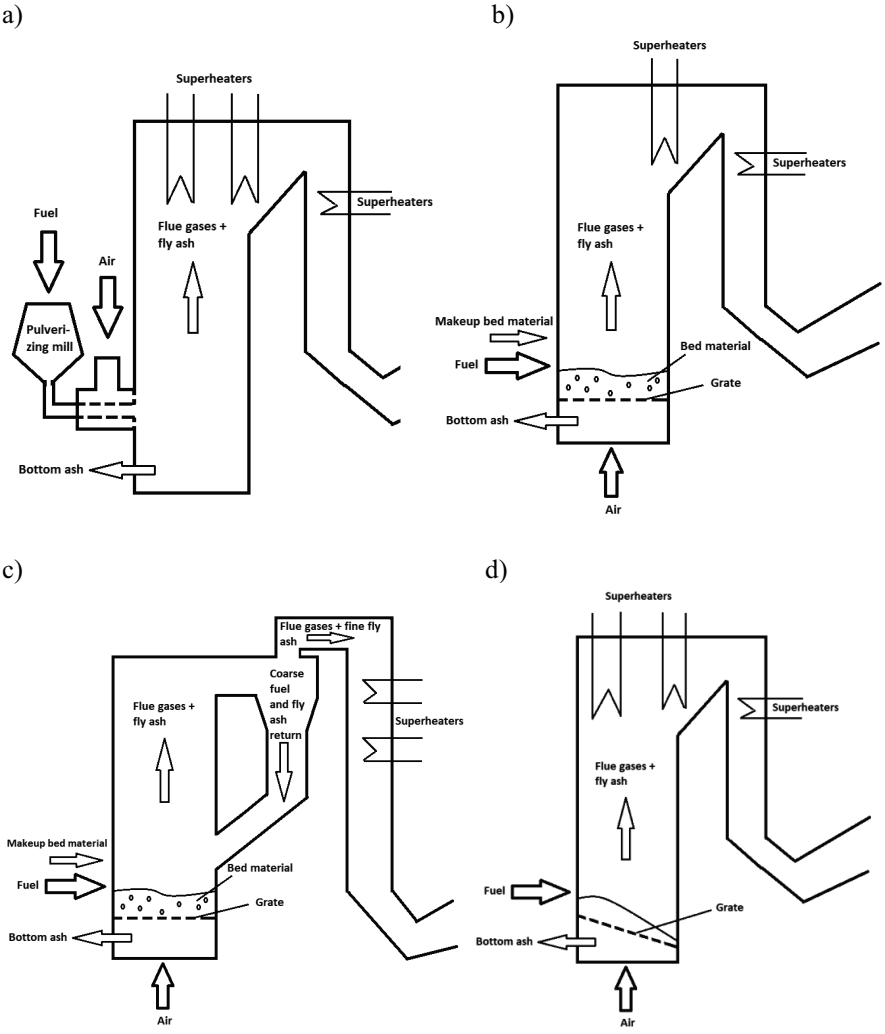

Figure 3. Schematics of different types of boilers. [a)]Pulverized fuel (PF) boiler; [b)]bubbling fluidized bed (BFB) boiler; [c)]circulating fluidized bed (CFB) boiler; and [d)]grate firing boiler.

In a modern boiler, the furnace walls are constructed with a double-wall structure. The side facing the fire is covered with ceramic refractory bricks. The water boiling tubes are located behind the refractory bricks (Blomberg, Hiltunen, & Makkonen, 2001). The heat of the flame in the furnace is transferred mostly by radiation and convection first to the refractory layer and then by conduction to the membrane wall tubing, where it boils the water. The saturated steam-water mixture then rises to the

steam drum. At the steam drum, larger water droplets are separated from the steam, moving to the bottom of the drum by gravitation. From the top of the drum, saturated steam is then directed to the superheaters, where it dries and heats up to its final temperature before flowing to the turbine.

2.3 Convection superheaters

Superheating of the steam before the turbine inlet is used for two reasons. First of all, as explained previously, increasing the steam temperature increases the thermal efficiency of the Rankine cycle. Secondly, superheating prevents droplet formation during the cooling of the steam temperature when being expanded in the turbine stages. In principle, the steam turbine could also be driven by high pressure saturated steam, but the small aerosol droplets that saturated (wet) steam contains tend to erode the turbine blades and guiding vanes during its path through the turbine and cause excessive turbine wear (Hesketh & Walker, 2005). Therefore, superheating the steam mitigates turbine steam path wear, but shifts the problem to the superheater fireside wear, because of the now increased metal surface temperatures. Superheaters are the most vulnerable parts to high temperature fireside corrosion. Maximum steam temperatures are over 500 °C in current units, with projections to over 600 °C in the future. Superheaters are used for the final temperature rise of the steam to its design value, and therefore they are the components with the highest metal surface temperatures (metal fireside surface temperature is determined mainly by the steam temperature). Furthermore, superheaters need to be also located at the high flue gas temperature area of the boiler in order to have sufficient ΔT between the fireside and steam side temperatures for efficient heat transfer. Some boiler designs have used superheaters located in furnace areas with a direct line of sight to the flame, thus utilizing radiation heat transfer as the prevailing heat transfer mechanism. However, radiation heat transfer superheaters are much more difficult to design than convection superheaters, and also the radiation load of the furnace fluctuates much more than the gas temperature in the convection section, which may lead to thermal shocks in the radiant superheaters and increased tube failures. Therefore, most of the boiler designs use only convection superheaters for final superheating.

Deposit formation on the furnace walls and equipment exposed directly in the furnace is called slagging, and deposit formation in the convection section is called fouling. There may be some similarities in certain aspects of the deposit formation mechanisms in both locations, but the division makes sense, because in slagging, inertial impaction of molten ash particles plays a more significant role because of the higher temperatures in the furnace. In fouling, the majority of the larger ash particles are solid, and the melt is formed – if it is formed – after condensation of alkali species. Corrosion under the superheater deposit is generally the most severe type of corrosion in biomass boilers. The partial pressures of gas-phase corrosive species in biomass combustion flue gases, HCl(g) and SO_2(g), are generally so low that they do not corrode the superheaters with gas-phase attack substantially. Therefore, an empirical rule-of-thumb law can be proposed: if there is no fouling, there is also a low corrosion rate. However, if there is fouling, there may be a low or a high corrosion rate of the underlying metal. The subject of this thesis concerns the fouling and corrosion chemistry in the convection superheaters in biomass-fired boilers.

3. Potassium behaviour in the boiler

Potassium has been found to influence slagging, fouling and corrosion behaviour in biomass-fired boilers. Chemical analyses of biomass fuels have revealed that the major difference compared to coal is the potassium content of the fuel. Concentrations of other elements that are considered risky in terms of ash-related problems – Na, Cl, S and heavy metals – are typically found in similar or lower levels than in coals, and therefore potassium behaviour during the thermal utilization of biomass has been studied extensively (Wei, Schnell, & Hein, 2005).

3.1 Existence and binding of potassium in biomass fuels

Potassium is a major plant nutrient, essential for the growth of terrestrial biomass. Potassium is present both in an organic matrix and as simple water soluble salts in biomass. In the lignocellulosic matrix, potassium can be bound in oxygen-containing functional groups, such as alkoxy, phenolic and carboxyl groups. As salts, it can be found dissolved in the water-containing matrix as KNO_3, KCl, KOH, K_2CO_3 or K_2SO_4 (Chen, Luo, Yu, Wang, & Zhang, 2017; Frandsen, et al., 2007; Boström, et al., 2012).

3.2 Release of gaseous potassium species from the fuel particle during pyrolysis and combustion

Combustion of solid fuel is typically divided into three stages: drying, devolatilization and char oxidation. During these phases, the biomass particle experiences a temperature history that triggers the reactions of potassium within the particle, and as the temperature increases, the evaporation of potassium compounds from the burning particle occurs. In the initial stages of combustion, water is evaporated from the particle. Because of the highly endothermic evaporation thermodynamics of water, the particle temperature stays fairly low (< 200 °C). In this stage, the potassium bound to the organic matrix remains intact, whereas the potassium salts contained in the water-containing part are left as salt residues within the biomass particle. At this stage, there is negligible release of potassium to the gas phase. After most of the water is released, devolatilization and combustion of hydrocarbons released from the biomass particle result in an increase in the gas temperature surrounding the particle. Heat transfer from the surrounding gas to the biomass particle induces a temperature gradient within the biomass particle. Typical surface temperatures are 1000-1100 °C, and particle core temperatures can still be less than 200 °C (if the core is still in the drying stage) (Mason, Jones, Darvell, & Williams, 2017). The high temperature within the particle triggers the breakdown of the organic matrix and the release of the organically bound potassium. The released potassium undergoes secondary reactions with the organic matrix and catalyses its decomposition. Simultaneously, potassium salts start evaporating from the particle. In the late stages of the devolatilization phase and during the char oxidation phase, the organic matrix containing potassium can be considered to be fully decomposed, and the final release of potassium to the gas phase is caused by the evaporation or decomposition of potassium salts (KCl, KOH, K_2CO_3, K_2SO_4). During char oxidation, the particle temperature is fairly isothermal, typically 1000 - 1100 °C, and the evaporating potassium can react with the minerals in the

ash. How much of the total potassium is finally released to the gas phase depends heavily on the ash chemistry. SiO_2 and Al_2O_3 and P_2O_5 are known to react with potassium compounds at these temperatures, forming K_2O-SiO_2, K_2O-SiO_2-Al_2O_3 or K_2O-SiO_2-P_2O_5 silicates retaining potassium in the ash and reducing gas-phase potassium release (Aho & Silvennoinen, 2004; Davidsson, Åmand, & Leckner, 2007; Niu, Yanqing, Tan, & Hui, 2016).

Figure 4 presents a summary of total potassium release from several references. The total K concentration can be easily measured by atomic absorption spectrometry or, if the flame temperature is high enough, with atomic emission spectroscopy using the atomic K spectral lines. However, determining the chemical form of the different gaseous K compounds is challenging.

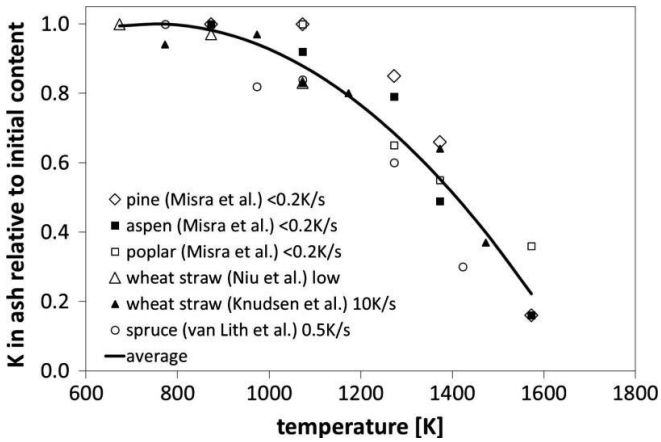

Figure 4. Release of K from different biomass fuels as a function of combustion temperature. Reproduced from (Mason, Darvell, Jones, & Williams, 2016). Licensed under a Creative Commons Attribution 4.0 Unported Licence.

Mass spectrometric studies on the release of potassium compounds from biomass at 1100 °C have revealed K^+, KCl^+ and KOH^+ as the main ions detected from the fume of potassium compounds released to the gas phase. The K^+ ion was the major component. However, Dayton concluded that the K^+ signal is most likely not an indication of potassium release in the elemental form, but is a result of the fragmentation of KCl(g) to K^+ and Cl^- during the ionization step in the mass spectrometer. Unfortunately, only the positive ions were detected in the experiments, and thus it is still unclear if the K^+ was an indication of elemental K-release or a fragment ion from KCl(g) or KOH(g) (Dayton, C., French, & Milne, 1995; Dayton, Frederick, & James, 1996). Photo-fragmentation ionization and atomic absorption spectroscopy measurements can distinguish between the different potassium species released in the gas phase. Sorvajärvi and colleagues showed that the proportion of elemental K is only minor, and most of the potassium is released as KOH(g) with low chlorine fuels and as KCl(g) with high chlorine fuels (Sorvajärvi, DeMartini, Rossi, Toivonen, & Juha, 2014). Furthermore, the high reactivity of elemental potassium should result in secondary reactions with OH* radicals or $HCl/SO_2/SO_3$ in the vicinity of the biomass particle, forming KOH(g), KCl(g) or K_2SO_4(g). Therefore, in practice, one can assume that the final release of potassium from the burning biomass particle is governed by the vaporization of KCl(s,l) and KOH(s,l). Recently, broad-band UV absorption spectrometry has also been shown to be able to measure gas-phase KCl(g) and

KOH(g) in the flame simultaneously (Weng, et al., 2019).

3.3 Transformations of gaseous potassium species in the boiler

The released KOH(g) and KCl(g) in the furnace section of a boiler undergo secondary reactions during their path through the boiler (Wang, et al., 2018; Wang, et al., 2018). The residence times of gas through a boiler are in the range of 2-3 s. During this time period, the gas is cooled from approximately 1000-1500 °C in the furnace to 100-150 °C at the chimney. In spite of the short residence time, the assumption that the gas phase reaches thermodynamic equilibrium is a good starting point for estimating the stable potassium compounds at each temperature range within the boiler (Boström, et al., 2012; Otsuka, 2008; Nutalapati, Gupta, Moghtaderi, & Wall, 2007; Hupa, 2005; Hupa, Karlström, & Vainio, 2017; Hupa, 2012). Kinetic restrictions are mainly present in the homogeneous nucleation steps or in heterogeneous reactions after the potassium species have condensed on surfaces that are at lower temperatures than the gas phase. Secondary reactions of KCl(s,l,g) and KOH(s,l,g) happen mostly in the superheater area of the boiler at gas temperatures of 400-1000 °C and metal temperatures of 400-600 °C (Jiménez & Ballester, 2004; Jiménez & Ballester, 2007; Westberg, Byström, & Leckner, 2003).

3.3.1 Gas-phase reactions

The following overall gas-phase reactions are likely for the released KCl(g) and KOH(g):

$$2KOH(g) + SO_2(g) + \tfrac{1}{2}O_2(g) \Leftrightarrow K_2SO_4(g) + H_2O(g) \quad (R1)$$

$$2KOH(g) + SO_3(g) \Leftrightarrow K_2SO_4(g) + H_2O(g) \quad (R2)$$

$$2KCl(g) + SO_2(g) + \tfrac{1}{2}O_2(g) + H_2O(g) \Leftrightarrow K_2SO_4(g) + 2HCl(g) \quad (R3)$$

$$2KCl(g) + SO_3(g) + H_2O(g) \Leftrightarrow K_2SO_4(g) + 2HCl(g) \quad (R4)$$

$$KOH(g) + HCl(g) \Leftrightarrow KCl(g) + H_2O(g) \quad (R5)$$

$$2KOH(g) + CO_2(g) \Leftrightarrow K_2CO_3(g) + H_2O(g) \quad (R6)$$

It should be noted that only KOH(g) reacts readily with $CO_2(g)$, whereas both KCl(g) and KOH(g) can react with $SO_2(g)$ or $SO_3(g)$. This is because of the thermodynamic stability of the potassium compounds, which follow the trend of K_2SO_4 > KCl > K_2CO_3 > KOH. It is also worth mentioning that these reaction equations present overall reactions only, and the detailed reaction mechanism of each reaction can be very complicated, involving tens of elementary reaction steps.

3.3.2 Homogeneous nucleation

In parallel to reactions R1-R6, homogeneous nucleation may take place according to:

$KOH(g) \Leftrightarrow KOH(s,l)$ (R7)

$KCl(g) \Leftrightarrow KCl(s,l)$ (R8)

$K_2SO_4(g) \Leftrightarrow K_2SO_4(s,l)$ (R9)

$K_2CO_3(g) \Leftrightarrow K_2CO_3(s,l)$ (R10)

Cooling of the flue gases drives the nucleation. Lowering the temperature also lowers the saturation vapour pressure, and at some point, the partial pressure in the flue gases reaches the saturation vapour pressure of the particular potassium compound, driving the gas-to-liquid or gas-to-solid phase change. Nucleation requires supersaturation of the nucleating compound:

$$S = \frac{p_i}{p_i(sat)} \geq 1 \quad (1)$$

where S = saturation ratio
p_i = partial pressure of the component in the flue gases
$p_i(sat)$ = saturation vapour pressure of the component

Purely homogeneous nucleation is rarer than heterogeneous nucleation, as it is energetically less favourable and therefore requires higher saturation ratios than heterogeneous nucleation. However, it is possible, and has been verified by laboratory tests concerning K_2SO_4(s), KCl(s) and K_2CO_3(s) nucleation when feeding KCl(aq) or KOH(aq) solution in gas flames (Weng, et al., 2018), (Mortensen, Hashemi, Wu, & Glarborg, 2019). Homogeneous nucleation of KOH(g) in combustion gases has rarely been reported. This may be related to the experimental difficulties in sampling of the KOH(s,l) aerosols. KOH(s,l,g) is a very reactive compound and will easily react according to R2, R5, R6, when the flue gases are cooled in the sampling line. This may lead to erroneous aerosol composition at the impactor stages compared to the initial composition in the flue gases (Jiménez & Ballester, 2005).

3.3.3 Heterogeneous nucleation

Heterogeneous nucleation on surfaces is the most common mechanism for nucleation. In a purely homogeneous system, the gas molecules need to collide in the gas phase first in two molecule collisions, and then these dimers need to collide with more molecules enough times to reach a critical nucleus size. If the critical nucleus size is not reached quickly enough, the embryos that are smaller than the critical nucleus size break down spontaneously because of entropy, and nucleation is delayed until a sufficiently high supersaturation ratio is reached.

3.3.3.1 Condensation on surfaces

A foreign surface in the system acts as a collision template on which the nucleating gas molecules collide, increasing the probability of collisions (because the surface is larger than a single molecule) and giving the nucleating molecules more time to interact (surface residence time between adsorption and desorption), thus lowering the free energy barrier for nucleation. Therefore, any surfaces in contact with the flue gas (ash particles, heat transfer surfaces) promote heterogeneous nucleation over homogeneous nucleation. However, in reality, both mechanisms have been proposed to happen in the flue gas flow of a boiler, with $K_2SO_4(s,l)$ nucleating first because of its lowest saturation vapour pressure among the potassium compounds in R7-R10.

3.3.3.2 Surface reactions without condensation

Heterogeneous nucleation on surfaces can happen even without supersaturation, if a chemical reaction takes place on the surface:

$$2KOH(g) \Leftrightarrow 2KOH(ads.) + SO_2(ads.) + \tfrac{1}{2}O_2(ads) \Leftrightarrow K_2SO_4(s,l) + H_2O(g) \quad (R11)$$

$$2KOH(g) \Leftrightarrow 2KOH(ads.) + SO_3(ads.) \Leftrightarrow K_2SO_4(s,l) + H_2O(g) \quad (R12)$$

$$2KCl(g) \Leftrightarrow 2KCl(ads.) + SO_2(ads.) + \tfrac{1}{2}O_2(ads.) + H_2O(ads.) \Leftrightarrow$$

$$K_2SO_4(s,l) + 2HCl(g) \quad (R13)$$

$$2KCl(g) \Leftrightarrow 2KCl(ads.) + SO_3(ads.) + H_2O(ads.) \Leftrightarrow K_2SO_4(s,l) + 2HCl(g) \quad (R14)$$

$$KOH(g) \Leftrightarrow 2KOH(ads.) + HCl(ads.) \Leftrightarrow KCl(s,l) + H_2O(g) \quad (R15)$$

$$KOH(g) \Leftrightarrow 2KOH(ads.) + CO_2(ads.) \Leftrightarrow K_2CO_3(s,l) + H_2O(g) \quad (R16)$$

where (ads.) means adsorbed molecules on a surface.

It is important to notice that in case of a surface reaction without condensation (above dew point), adsorbed intermediate species (ads.) in these equations refer to a single molecular monolayer of material (Langmuir type of adsorption) (Steinberg & Schofield, 2002; Schofield, 2003).

3.3.3.3 Surface reactions with condensation

Below the dew point of the potassium compound in the flue gas (Figure 5), adsorption can continue without the need for chemical reaction to capture the molecules on the surface. The reaction equations are the same as without condensation (R11-R16), but now the adsorbed species refer to multi-monolayer adsorption forming a macroscopic phase that is either liquid or solid depending on the temperature of the surface. If the surface reaction proceeds through condensation, the condensed potassium compound can form a liquid phase that may increase corrosion of the underlying surface. This is especially important in the case

of KOH, which has a low melting point of 406 °C compared to KCl (773°C), K_2CO_3 (891°C) and K_2SO_4 (1069 °C). Most early work has studied Na_2SO_4 nucleation on hot surfaces due to its importance in deposit formation in coal-fired boilers and on gas turbine blades when the inlet air or fuel contains sodium as an impurity (Rosner, Daniel, & Liang, 1988; D.E. & Nagarajan, 1987). The sodium content of biomass is normally very low, and therefore K_2SO_4(s,l) formation by condensation of KCl(g) and KCl(s,l) sulphation after condensation (R13, R14) has been studied extensively more recently (Nielsen, Frandsen, Dam-Johansen, & Baxter, 2000; Sengelov, et al., 2013).

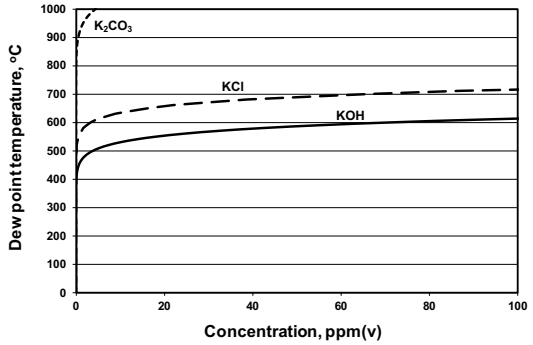

Figure 5. Calculated equilibrium dew points for the gaseous potassium compounds (from publication III). Reprinted from Materials and Corrosion, Copyright (2011) Wiley-VCH Verlag GmbH & Co. KGaA. Reproduced with permission.

3.3.4 Effect of reducing conditions (gasification)

In gasification or combustion in sub-stoichiometric oxygen contents, the major difference concerning potassium chemistry is the form of sulphur and carbon in the flue gases. Sub-stoichiometric regions in the boiler are used in low NO_x combustion, where the low oxygen content and combustion temperature are used to minimize the direct reaction of N_2 with O_2 in the furnace. In reducing conditions, sulphur is not oxidized to SO_2(g) and SO_3(g) in the flue gases, but is present as H_2S(g) or COS(g), and carbon is present as CO(g) instead of CO_2(g). This changes the potassium chemistry:

$$2KOH(g) + H_2S(g) \Leftrightarrow K_2S(g) + 2H_2O(g) \quad \text{(R17)}$$

$$2KCl(g) + H_2S(g) \Leftrightarrow K_2S(g) + 2HCl(g) \quad \text{(R18)}$$

$$2KOH(g) + CO(g) \Leftrightarrow K_2CO_3(g) + H_2(g) \quad \text{(R19)}$$

K_2S may further condense out of the flue gases on surfaces or nucleate homogeneously to aerosols:

$$K_2S(g) \Leftrightarrow K_2S(s,l) \quad \text{(R20)}$$

In addition to changing the thermodynamically stable form of the potassium-sulphur compounds, the thermodynamic driving forces in reactions R17-R19 are

also substantially lower than in reactions R11-R14 and R16. Therefore, in gasification, the equilibrium for the stable potassium compounds is more on the KCl(g) and KOH(g) side than in the case of combustion. This reduces the effectiveness of gaseous alkali capture by sulphur addition, a technique frequently used to mitigate fouling and corrosion problems (Davidsson, Åmand, & Leckner, 2007; Lind, et al., 2006).

4. Physicochemical view of fouling of the superheaters

Figure 6 shows a schematic figure of the major deposit formation mechanisms around a superheater tube. Larger ash particles have enough inertia that they do not follow the streamlines of gas around the superheater tube, whereas vapours and the smallest aerosol particles are deposited by diffusional and thermophoretic forces. Therefore, a typical deposit structure is heterogeneous, with an inner layer next to the metal surface having fairly uniform thickness around the tube, and an outer layer that is thicker at the leading edge of tube, where the inertial impaction rate is highest.

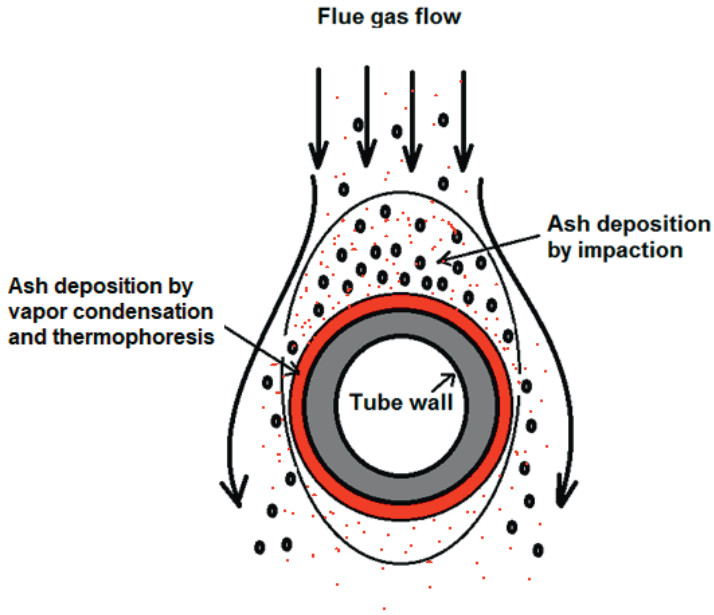

Figure 6. Schematic figure of the major deposition mechanisms around a superheater tube. The layer coloured in red is formed by heterogeneous condensation of alkali compounds on the metal surface and by thermophoresis of the smallest alkali aerosol particles (red dots) formed by homogeneous nucleation in the flue gases.

4.1 Condensation of alkali species

Fouling of the heat transfer surfaces is initiated with gas-phase condensation reactions. Potassium compounds condense on the cooler surfaces according to reactions R7-R16, forming KOH-K_2CO_3-KCl-K_2SO_4 condensate. Analog reactions

are valid for sodium, too, so in case the feedstock contains Na in addition to K, the condensate is NaOH-Na_2CO_3-NaCl-Na_2SO_4-KOH-K_2CO_3-KCl-K_2SO_4 (black liquor, waste biomass). The initial condensation layer acts as a glue layer capturing the larger ash particles and aerosols. The initial layer may be solid or liquid depending on its composition (Otsuka, 2008; Tran, Gonsko, & Mao, 1999).

4.2 Deposition of alkali aerosols by thermophoresis

Gases and the smallest aerosol particles experience a thermophoretic force driven by the temperature gradient between the flue gases and the superheater tube. In the case of gases, this is normally referred to as thermal diffusion or Soret diffusion, and in case of particles, as thermophoresis (Geelhoed, Westerweel, Kjelstrup, & Bedeaux, 2008). For gases, Fick's diffusion driven by the concentration gradient between the gas and the surface of the tube dominates the deposition rate, but for aerosols, the ratio of the thermal diffusion to Fick's diffusion increases (Soret coefficient), and the thermophoretic mechanism may be significant. The thermophoretic diffusion constant is inversely proportional to the size of the particle:

$$S_T = \frac{D_T}{D_m}, \quad D_T = \frac{kT}{3\pi\eta d} \tag{2}$$

S_T = Soret coefficient
D_m = mass diffusion coefficient
D_T = thermal diffusion coefficient
T = temperature
k = Boltzmann's constant
η = dynamic viscosity of the fluid
d = particle diameter

Therefore, this effect becomes negligible for massive particles, which deposit by the inertial impaction mechanism. The particle size distribution of the fly ash particles in biomass-fired boilers is typically bimodal, with one peak appearing at $d \approx 100$ nm, and the other at $d > 1$ µm. The peak at smaller d values is due to the homogeneous nucleation of gaseous alkali compounds, and the particles with $d > 1$ are considered to represent the particles formed from mechanical attrition processes within the boiler. The composition of the larger particles is typically similar to bulk ash composition of the fuel. These larger particles act as nucleation centres, onto which heterogeneous nucleation and surface reactions of alkali species is possible (R11-R16, R20) (Jiménez & Ballester, 2004; Wiinikka, Rikard, Boman, Boström, & Öhman, 2007).

4.3 Melting point of the alkali deposit as a function of its composition

The melting point of the deposit layer is an important parameter to predict the fouling and corrosion propensity. A substantial amount of work has been done to predict the melting point of the Na_2S-Na_2CO_3-NaCl-Na_2SO_4-K_2S-K_2CO_3-KCl-K_2SO_4 system as a function of its composition (Lindberg, Backman, & Chartrand, 2007). This system is of interest in the fouling and corrosion prediction in recovery

boilers, but it is also relevant in biomass-fired boilers. The major compositional difference between recovery boiler deposits and biomass boiler deposits is that sodium is the dominant alkali in the former, and potassium in the latter. The range of melting temperatures determined both experimentally and with thermodynamic calculations of the Na_2S-Na_2CO_3-NaCl-Na_2SO_4-K_2S-K_2CO_3-KCl-K_2SO_4 system has been found to be 500-800 °C (Tran, Gonsko, & Mao, 1999; Backman, Enestam, & Zevenhoven, 1998; Backman, Hupa, & Uppstu, 1987; Honghi, Mao, & Chartrand, 2009). The system does not melt abruptly at one particular temperature, but is characterized by an initial melting point, T_0, followed by an increase in the fraction of melt in the system with increasing temperature and finally complete melting. Characteristic temperatures have been proposed as fouling predictors: T_{15} and T_{70}, where T_{15} is the so-called "sticky temperature" and refers to the temperature where the fraction of melt is 15%. Similarly, T_{70} is called the "flow temperature" and indicates the temperature where the fraction of melt is 70% (Backman, Hupa, & Uppstu, 1987). This classification was developed for recovery boilers, where the liquor ash particles are composed almost entirely of alkali salts and therefore the larger particles deposited by impaction are also partially or fully molten. In biomass-fired boilers, the larger ash particles consist of K-Ca-Al-silicates and are typically solid at the superheater area in the convection section. Therefore, their tendency to stick when impinging the tube surface is likely to be more dependent on the stickiness of the condensed layer on the tube, rather than the stickiness of the particle itself (Zbogar, Frandsen, Jensen, & Glarborg, 2009). However, the melting point predictions of the Na_2S-Na_2CO_3-NaCl-Na_2SO_4-K_2S-K_2CO_3-KCl-K_2SO_4 system are still useful for biomass boiler deposits, as well. The effects of KOH and NaOH on the melting point of the deposits have not been extensively studied. It has been assumed that the alkali hydroxides have reacted to alkali carbonates before depositing on the tube surfaces. However, the correctness of this assumption depends on the flue gas temperature. Alkali hydroxide–alkali carbonate equilibrium is heavily dependent on temperature, as shown in Figure 7. Tube surface temperatures are typically 400-600 °C in the superheaters, which is low enough for carbonates to be stable. One must, however, consider the continuous nature of deposit formation in the boilers, where the flue gas provides a continuous flux of alkali compounds condensing on the tube. Therefore, in the case of hydroxides, the condensing flux of alkali hydroxides may form carbonates only after first impinging the tube surface. The KOH-NaOH system has a eutectic temperature as low as 170 °C with 406 °C and 323 °C melting points for pure KOH and NaOH. Therefore, if the hydroxides are taken into account in the melting point prediction, one can assume the system to have T_0 values below 200 °C, resulting in predictions of a continuous molten phase on the superheater tube surfaces.

a) b)

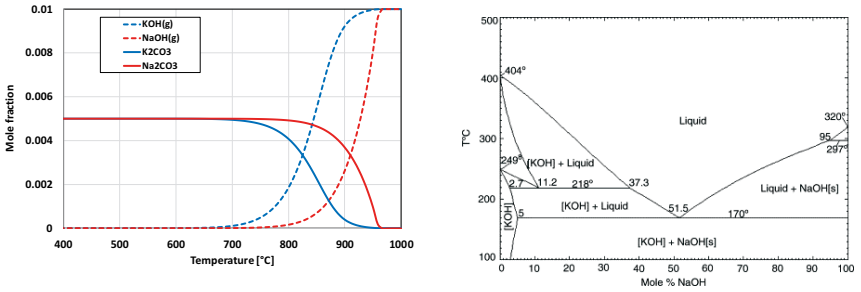

Figure 7. [a](Na,K)OH(g)-(Na,K)$_2$CO$_3$(s) equilibrium in the flue gases calculated with HSC v.6.12; [b]Phase diagram of the KOH-NaOH system (Zhuang & Edgar, 2005), with permission from Elsevier.

4.4 Deposition of larger ash particles by inertial impaction on sticky surface

Recent research has explored the mechanisms of deposit shedding. The long-term deposit formation rate is determined by the accumulation and shedding rates of the deposits. In large-scale boilers, automatic shoot blowing equipment is typically used to remove the formed deposits periodically. Therefore, not only the deposit formation rate, but also the tenacity of the formed deposits determine the long-term fouling problems in the boiler. Loose deposits that are easily removed by soot blowing are non-problematic, even if the deposit formation rate is high. In order to predict if the ash particle is stuck or rebounded at collision depends both on the viscosity of the particle and on the viscosity of the capturing surface (Zbogar, Frandsen, Jensen, & Glarborg, 2009). The viscosity depends on the melt fraction of the alkali layer on the tube, and therefore the melting behaviour of the condensation layer is again an important parameter determining the capture efficiency of the surface. The molten layer next to the metal surface also increases the corrosion rate between the deposits and the tube, which increases the adhesion of the deposit layer towards the superheater tube and makes it more difficult to be removed by soot blowing (Laxminarayan, et al., 2018).

5. High temperature corrosion under alkali deposits

The deposits formed on the heat exchanger surfaces provide a formation of a local environment that can be, chemically, very aggressive towards the protective oxides formed on the steel surfaces. Superheaters are expected to last more than 100,000 service hours in coal-fired power plants. In biomass firing units, the lifetime can be as low as 20,000 service hours, if high steam temperatures are used (Henderson, Szakálos, Pettersson, & Högberg, 2006). Several possible mechanisms are responsible for the corrosion damage, but it has been argued that alkali salt corrosion is the most relevant in biomass firing units. The alloys used in the superheaters are normally designed to withstand gas-phase oxidation quite well. Also, the gaseous HCl(g) and SO_2(g)/SO_3(g) levels in the flue gases are generally rather low when burning virgin biomass. However, with waste biomass or agricultural residues, the HCl(g) concentration in the flue gas can be high enough to cause severe corrosion by purely gas-phase attack. In many cases, several

corrosion mechanisms operate simultaneously, making the optimization of the alloy composition a challenging task.

4.1 Gas-phase oxidation

The most common and the most studied corrosion mechanism of metals is gas-phase oxidation by O_2(g). Oxidation of metals is a natural process, driven by the high thermodynamic stability of metal oxides. Apart from the noble metals, metals in their elemental form are not thermodynamically stable. Therefore, the protection of the base metal in structural alloys in oxidizing environments relies on the formation of a thin, dense metal oxide layer on the surface of the alloy. This oxide layer acts as a diffusion barrier for the diffusion of O_2(g) from the environment deeper into the alloy or for the diffusion of metal atoms from the bulk of the metal to the surface of the oxide (inward-growing or outward-growing oxide scale). In order to function as a proper barrier, the formed oxide should be low in microscopic and macroscopic defects, as the diffusion of atoms in solids is typically fastest through lattice defects or grain boundaries (Young, 2016). Chromium is the most common element added to the alloy to reduce its oxidation rate. When a certain threshold content of chromium is present in an Fe-Cr alloy, the chromium atoms diffuse preferably over Fe atoms to the surface of the alloy and form a protective Cr_2O_3 oxide on the surface. The minimum amount of Cr to form a protective Cr_2O_3 layer is approximately 12 at-% for ferritic (BCC) steels and 17 at-% for austenitic (FCC) steels, depending a bit on the other constituents in the alloy that modify the diffusion rate of Cr within the alloy and the oxide scale. If the Cr content is lower in a binary Fe-Cr alloy, the formed oxide is no longer essentially pure Cr_2O_3, but a solid solution in the form $Cr_{2-x}Fe_xO_3$ where x = 0 - 2, or a spinel oxide in the form of $Fe_{3-x}Cr_xO_4$, where x = 1.5 - 2 (Tsai, Huntz, & Dolin, 1996; Cabrera & Mott, 1949).

In the case of more complicated alloys that contain other major alloying elements, this protective oxide can also contain Ni or Co, for example. Furthermore, the protective oxide composition may change when going deeper into the alloy. The oxygen activity is highest at the topmost surface of the alloy, gradually lowering with the depth of the diffusion zone. Therefore, the cross-section of a protective oxide layer typically contains the highest metal oxidation state compounds at the surface of the alloy and lower oxidation state compounds deeper in the layer. For example, in case of pure iron oxidized isothermally at > 570 °C, the oxide formed results in a scale structure of Fe_2O_3-Fe_3O_4-FeO-Fe, reflecting the oxygen activity in the diffusion zone from the surface to the bulk metal (Young, 2016). In case of multi-component alloys, not only oxidation state segregation, but also oxide segregation within the protective oxide scale can take place, forming a multilayer structure with different metal oxides layered on top of each other. This multilayer oxide scale formation is driven by the solubility limits of different alloying elements in the base oxide scale, by the differences in the thermodynamics of oxidation and by the differences in the diffusion coefficients of different atoms within the alloy and the scale. When trying to predict which oxide forms on the surface of an alloy, a good starting point is to look at the Ellingham diagram shown in Figure 8, which shows the Gibbs free energy of oxide formation as a function of temperature and oxygen partial pressure (Ellingham, 1944).

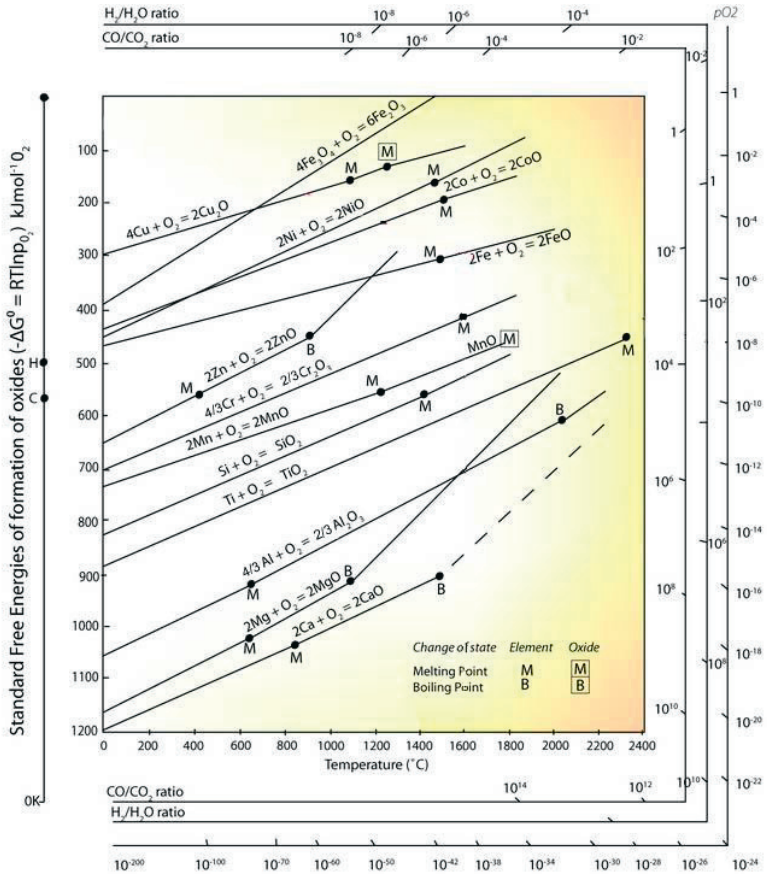

Figure 8. Ellingham diagram of common protective oxides. © 2004-2018 University of Cambridge. Creative Commons Attribution-NonCommercial-ShareAlike 2.0 UK: England & Wales License

In addition to Cr, aluminium is the other common element used to improve the oxidation resistance of the alloys. Al_2O_3 forms even more preferably than Cr_2O_3, also forming a good quality protective oxide. Al_2O_3-forming alloys are usually used in the highest service temperature conditions. Al_2O_3-forming alloys are not used commercially in the construction of superheater tubes, because binary Fe-Al alloys have poorer oxidation resistance than Fe-Cr alloys in the intermediate temperature range (400-600 °C) where the superheater surfaces typically operate. Tertiary FeCrAl or FeNiAl alloys provide superior oxidation resistance over the entire temperature range, but are much more expensive than Fe-Cr alloys and therefore not typically used as the tube material. However, Fe-Al, Ni-Al, Fe-Cr-Al or Ni-Al-Cr coatings on the load-bearing Fe-Cr tubes can be used to increase the corrosion resistance of the superheater tubes (Stringer & Wright, 1995).

In addition to O_2(g) as the oxidising species, combustion flue gases always contain significant partial pressures of H_2O(g). H_2O(g)-induced oxidation of alloys is much less understood than O_2(g)-induced oxidation. It has been reported that oxidation can be much more rapid in H_2O(g)-containing environments compared to dry O_2(g) atmosphere. For Cr_2O_3-forming alloys, the formation of chromium oxyhydroxide ($CrO_2(OH)_2$(g)) has been suggested to cause the higher corrosion rate in high temperature wet conditions. The saturation vapour pressure of

$CrO_2(OH)_2$(s,l) becomes significant at high temperatures and H_2O(g) partial pressures, and leads to the evaporation of Cr from the alloy, thus increasing the corrosion rate. However, it must be emphasized that the surface temperatures in question in the superheaters (400-600 °C) and H_2O(g) partial pressures (0.05-0.30 bar) are too low for the $CrO_2(OH)_2$(s,l) evaporation alone to explain the high fireside corrosion rates in actual service conditions in biomass-fired boilers (Young & Pint, 2006; Pettersson, Folkeson, Johansson, & Svensson, 2011).

5.2 Gas-phase corrosion with sulphur species (sulphidation)

In atmospheres where gas-phase sulphur activity is high and oxygen activity low, alloys can react directly with the gas-phase sulphur compounds, forming metal sulphides. This type of environment is typical, for example, in gasification flue gases or in fluid catalytic cracking units in the oil refining industry. Liquid phase sulphidation involves reactions of molten sulphur salts with the alloy and is discussed in the molten phase corrosion section of this thesis (section 5.4). The major gas-phase compounds responsible for sulphidation corrosion are H_2S(g) and SO_2(g)/SO_3(g). When reacting with the alloy surface, they form a defective metal sulphide, sulphite or sulphate scales that provide inferior diffusion barrier properties compared to pure metal oxide scales. Therefore, the diffusion rates through the scale are higher than in scales formed in a purely oxidising atmosphere, which results in higher corrosion rates. Alloying with Cr is generally a strategy to reduce corrosion in sulphur-containing environments because of the high quality protective oxide it forms and its preferable affinity to oxygen versus sulphur, as shown in Figure 9 (Ellingham, 1944; Mrowec & Przybylski, 1985).

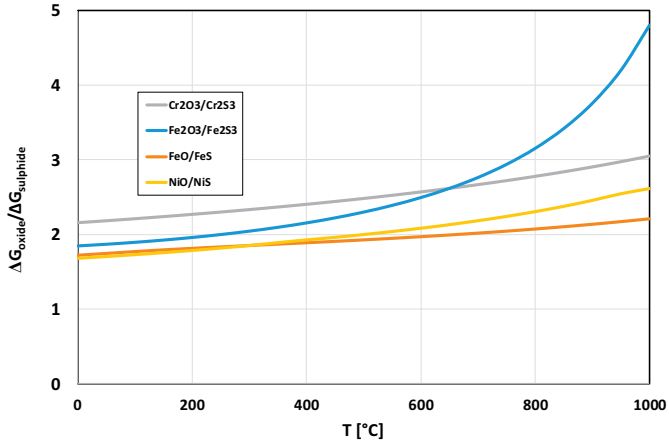

Figure 9. Relative stability of metal oxides over metal sulphides for the major steel components. Calculated with HSC v6.12.

5.3 Gas-phase corrosion with chlorine species (chlorination)

In addition to gas-phase sulphur compounds, the combustion flue gases in many cases also contain chlorine compounds. Waste-based biomass in particular typically contains high concentrations of chlorine in the feedstock. During combustion, the chlorine species are released into the gas phase as HCl(g), or if the feedstock also

contains significant amounts of alkali metals (Na, K) or heavy metals (Zn, Pb, Cu), the chlorine will combine with these elements, forming KCl(g), NaCl(g), $ZnCl_2$(g), $PbCl_2$(g), CuCl(g) or $CuCl_2$(g) (Ma, Terrence, Frandsen, Beibei, & Guanyi, 2020) With alkali and heavy metal chlorides, condensation on the superheater tubes and formation of a highly corrosive molten metal chloride phase on the tubes is possible if the condensate has a lower melting point than the tube surface temperature (Type 1 hot corrosion, discussed in section 5.4.5). HCl(g) or Cl_2(g) may corrode the superheater tubes by gas-phase reactions with the protective oxides, forming oxychlorides or diffusing through the cracks and defects in the protective oxide and reacting with the base metal (Grabke, Reese, & Spiegel, 1995; Cantatore, et al., 2019). With pure gas-phase attack by Cl_2(g) or HCl(g), corrosive chloride melt formation is also possible after an incubation period during which the metal chloride melt forms from the corrosion products between the Cl-bearing gases and the tube material (Type 2 hot corrosion, discussed in section 5.4.6). Melting points and stabilities of the chlorides of the basic steel components are presented in Table 1 and Figure 10. The relative stabilities of metal chlorides versus the metal oxides are higher than for the corresponding metal sulphides (Figure 9). In addition, the higher volatility and lower melting points of most metal chlorides compared to metal sulphides make chlorination corrosion generally more severe than sulphidation corrosion. Upon reaction with the corrosive chlorine species, the base metals of steel (Fe, Cr, Ni) form relatively stable and volatile chlorides, and the corrosion reactions involve vaporization of $FeCl_2$(g), $FeCl_3$(g), $CrCl_2$(g), $CrCl_3$(g), $NiCl_2$(g) or oxychlorides from the alloy, leading to vaporization of the tube material to the gas phase. However, it is worth emphasizing here that virgin biomasses (wood, agricultural biomass, energy crops) typically contain negligible amounts of heavy metals and do not always contain high chlorine concentrations, either. Therefore, the partial pressures of HCl(g), KCl(g), NaCl(g) or heavy metal chlorides in the flue gases are often very low (< 100 ppm(v)), and chlorination corrosion has been argued to be the major corrosion mechanism in many cases, whereas the corrosion may in fact have resulted from alkali corrosion.

Table 1. Comparison of the melting points and saturation vapour pressures of selected metal chlorides, oxychlorides, sulphides, sulphites and sulphates. d = decomposes, s = sublimates (Nielsen, Frandsen, Dam-Johansen, & Baxter, 2000; Budkuley & Patil, 1990; Salib, El-Maraghy, El-Wafa, & El-Sayed, 1989; CRC Handbook of Chemistry and Physics, 2004; Hultgren & Brewer, 1956)

Chlorides			Oxychlorides			Sulphides			Sulphites			Sulphates		
Compound	Melting point [°C]	Saturation vapor pressure at 500 °C [atm]	Compound	Melting point [°C]	Saturation vapor pressure at 500 °C [atm]	Compound	Melting point [°C]	Saturation vapor pressure at 500 °C [atm]	Compound	Melting point [°C]	Saturation vapor pressure at 500 °C [atm]	Compound	Melting point [°C]	Saturation vapor pressure at 500 °C [atm]
$NiCl_2$	1001	10^{-4}	FeOCl	300 (d)	-	NiS	797	10^{-24}	$FeSO_3$	200 (d)	-	$FeSO_4$	680 (d)	-
$CrCl_2$	824	10^{-3}	CrO_2Cl_2	-96.5	> 1	Cr_2S_3	1350		$NiSO_3$	240 (d)	-	$Fe_2(SO_4)_3$	480	
$FeCl_2$	677	10^{-5}	$VOCl_3$	-76.5	> 1	FeS	1194	10^{-23}	$Cr_2(SO_3)_3$	220 (d)	-	$Cr_2(SO_4)_3$	> 700 (d)	-
$CrCl_3$	1152	10^{-7}	WO_2Cl_2	265	> 1	Fe_2S_3	20 (d)	-	$CoSO_3$	200 (d)	-	$NiSO_4$	> 100	
$FeCl_3$	308	> 1	$WOCl_4$	211	> 1	CoS	1195	10^{-22}	$MnSO_3$	360 (d)	-	$CoSO_4$	735	
$CoCl_2$	735	10^{-6}	MoO_2Cl_2	100 (d)	-	MnS	1610	10^{-26}				$MnSO_4$	710	
$MnCl_2$	654	10^{-5}	$MoOCl_3$	310 (s)	> 1	MoS_2	1185	10^{-31}				$V_2(SO_4)_3$	400 (d)	-
VCl_2	1027	10^{-5}	$MoOCl_4$	105 (d)	-	WS_2	1250	10^{-36}						
VCl_3	> 300 (d)	-												
VCl_4	-24.5	> 1												
$MoCl_3$	410 (d)	-												
$MoCl_4$	552	> 1												
$MoCl_5$	194	> 1												
WCl_3	550	10^{-4}												
WCl_4	450	> 1												
WCl_5	248	> 1												
WCl_6	275	> 1												
$SiCl_4$	-68.7	> 1												

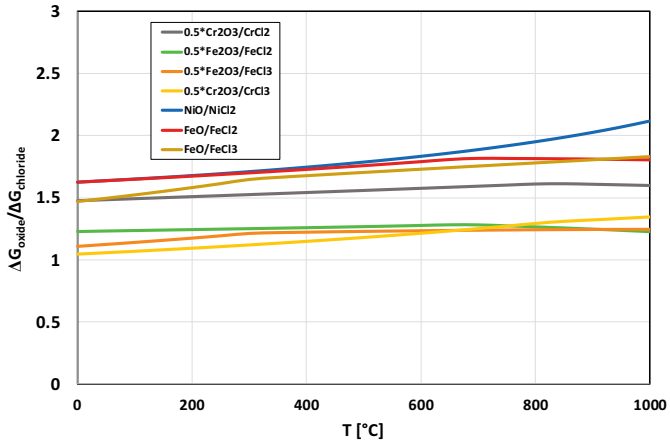

Figure 10. Relative stability of metal oxides over metal chlorides for the major steel components. Values are normalized to 1 mole of metal atoms. Calculated with HSC v6.12.

5.4 Molten-phase corrosion (hot corrosion)

Hot corrosion is a form of high temperature corrosion where the corrosive media is a molten salt formed on a component surface. This has been studied for more than half a century. The earliest studies on hot corrosion were aimed at understanding high temperature corrosion in combustion gas turbines and coal-fired power plants. These earlier works established a general understanding of hot corrosion, and it was found that hot corrosion can be considered as a high temperature analogue to aqueous corrosion (Stringer, 1977; Rapp, 2002; Hendry, 1980; Rapp & Otsuka, 2009). It can be considered as the most severe high temperature corrosion mechanism in combustion flue gases and can lead to superheater tube failure after less than a year of service life.

5.4.1 Type I and type II hot corrosion

Historically, hot corrosion was divided into two types: Type 1 and Type 2. The original definition of Type 1 corrosion was that it takes place at component surface temperatures higher than the melting point of the pure Na_2SO_4 salt. However, hot corrosion in the presence of vanadium impurities along with sulphur impurities that were encountered in heavy fuel oil-burning systems was still considered Type 1 hot corrosion. In these systems, the corrosion was caused by the Na_2SO_4-V_2O_5 salt mixture that exhibited a substantially lower melting point than pure Na_2SO_4, and therefore hot corrosion damage already started at substantially lower surface temperatures (Singh, Puri, & Prakash, 2007). Therefore, perhaps a broader definition of Type 1 hot corrosion in complex salt mixtures could be that it happens above the melting point of the deposit that has formed from the inorganic impurities originating from the fuel. Because Type 1 hot corrosion requires a molten deposit formation by condensation reactions, one can easily define the prerequisites for Type 1 hot corrosion to take place:

1. The component surface temperature has to be higher than the melting point of the condensing substance, or in the case of salt mixtures, higher than the minimum melting point of the salt mixture.

2. The component surface temperature has to be lower than the dew point of the condensing substance, or in the case of salt mixtures, lower than the dew point of the most volatile constituent in the salt mixture.

Using the criteria above, the surface temperature range where Type 1 hot corrosion is active is presented in Figure 11 for a number of possible salt systems formed on component surfaces during the combustion or gasification of biomass. Other salt mixtures are of course also possible, depending on the inorganic impurities found in the fuels. Type 2 hot corrosion takes place at surface temperatures below the melting point of the deposit. However, the corrosion reactions still involve molten salt as the corrosive media, but the melt formation may be local and is preceded by a solid–solid reaction between the component material and the deposit or a gas–solid reaction between the component material and corrosive gases (HCl(g), Cl_2(g), SO_2(g), SO_3(g), etc.) within the deposit. Because of the local melt formation, Type 2 corrosion morphology is often distinguishable as pitting corrosion rather than the uniform attack typical for Type 1 morphology. Because Type 2 hot corrosion requires a chemical reaction of the component construction material to form the melt, the criteria for Type 2 hot corrosion to take place is more difficult to define. The same dew point criteria that were used for Type 1 hot corrosion are not valid for Type 2, because the corroding construction material is continuously supplying a constituent to the melt.

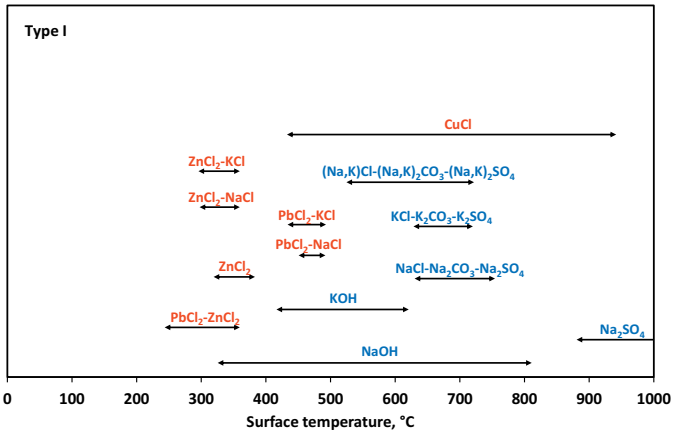

Figure 11. Examples of possible chemical systems involved in Type I hot corrosion in biomass-fired systems. The dew point (calculated with HSC v4.1) for 100 ppm(v) of the most volatile salt in the gas phase was used as the higher temperature limit and melting point of the salt as the lower (Nielsen, Frandsen, Dam-Johansen, & Baxter, 2000; Tran, Gonsko, & Mao 1999; CRC Handbook of Chemistry and Physics, 2004; Bankiewicz, Enestam, Yrjas, & Hupa, 2013; Bankiewicz, Yrjas, & Hupa, 2009). The red font colour refers to chemical systems that are important when firing contaminated biomass based fuels (waste), whereas the blue colour refers to uncontaminated biomass fuels (virgin biomass).

Even if this melt constituent were to have high saturation vapour pressure, it is difficult to predict if it would stay in the melt or evaporate from it, because the intermolecular forces in the mixed salt melt may substantially suppress its vapour pressure from the vapour pressure of the pure substance. However, an upper surface temperature limit can still be suggested as the dew point of the least volatile salt in the formed salt mixture. Therefore, the following criteria for Type 2 hot corrosion to take place is suggested:

1. The component surface temperature has to be higher than the minimum melting point of the salt mixture.

2. The component surface temperature has to be lower than the dew point of the least volatile constituent in the salt mixture.

Figure 12 presents some example salt systems that are important in biomass combustion and gasification systems. Alkali iron tri-sulphate, the main substance responsible for hot corrosion in coal-fired boilers (Harb & Smith, 1990) is also added to the figure for comparison, although in coal-fired boilers, the alkali iron tri-sulphate corrosion could also be considered Type 1 hot corrosion in some cases. This is because many coals contain pyrite (FeS) as an impurity, and therefore the iron in the deposits can also originate from the fuel. However, biomass fuels contain negligible amounts of iron impurities, and therefore, in biomass-fired systems the iron in the deposits must originate from the component construction materials. Therefore, it is more appropriate to categorize alkali iron tri-sulphate corrosion as Type 2 hot corrosion in these systems.

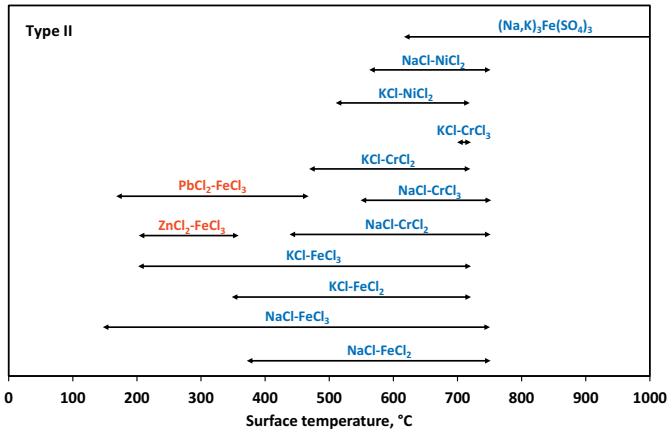

Figure 12. Examples of possible chemical systems involved in Type II hot corrosion in biomass-fired systems. The dew point (calculated with HSC v4.1) for 100 ppm(v) of the least volatile salt in the salt phase was used as the higher tempeature limit and melting point of the salt as the lower (Nielsen, Frandsen, Dam-Johansen, & Baxter, 2000; Tran, Gonsko, & Mao, 1999; CRC Handbook of Chemistry and Physics, 2004; Bankiewicz, Enestam, Yrjas, & Hupa, 2013; Bankiewicz, Yrjas, & Hupa, 2009) The red font colour refers to chemical systems that are important when firing contaminated biomass-based fuels (waste), whereas the blue colour refers to uncontaminated biomass fuels (virgin biomass).

5.4.2 Acid–base properties of molten salts

Molten salt chemistry literature uses the Lux–Flood definition of acidity–basicity. The theory defines an acid as an oxide ion (O^{2-}) acceptor and a base as an oxide ion donor. Instead of water as the electrolyte with H_3O^+ or OH^- ions participating in the corrosion reactions, in hot corrosion, the molten salt acts as the electrolyte, with O^{2-} ions participating in the corrosion reactions. Therefore, the hot corrosion mechanisms in oxyanion melts are generally explained as dissolution reactions of the protective metal oxides in the melt as a function of melt basicity $p[O^{2-}]$, again analogous to the dissolution of metals in water as a function of pH in aqueous corrosion. This interpretation works well with simple electrolytes containing O^{2-} as the main corrosive ion, with the most studied system being the pure Na_2SO_4 melt. However, recently, the ongoing switch from fossil fuels to renewable, biomass-based fuels has led to the formation of much more complicated salt mixtures on the combustion equipment surfaces, and therefore, more research is needed to understand the effects of additional constituents in the melt on the corrosion mechanisms of metals and ceramics (Lehmusto, Linddberg, Yrjas, Skrifvars, & Hupa, 2012), . For example, the synergetic effect of the Cl^- ion with the O^{2-} ion on corrosion is not well understood. Also, the role of cations (K^+, Na^+, Ca, etc.) in the corrosion reactions remains elusive (Karlsson, Pettersson, Johansson, & Svensson, 2012). The basicity scale of the melt is determined by the salt dissociation equilibrium, for example:

Reaction	Equilibrium basicity a 500 °C	
$2KOH \Leftrightarrow K_2O + H_2O(g)$	$p[K_2O] = 5.5$	(R21)
$K_2CO_3 \Leftrightarrow K_2O + CO_2(g)$	$p[K_2O] = 9.3$	(R22)
$2KCl + H_2O(g) \Leftrightarrow K_2O + 2HCl(g)$	$p[K_2O] = 10.9$	(R23)
$K_2SO_4 \Leftrightarrow K_2O + SO_3(g)$	$p[K_2O] = 18.3$	(R24)

Similar reaction equations can be written for Na. The O^{2-} ion is the actual basicity determining ion in the molten salt, but the equilibrium between the potassium or sodium oxide and their ionic forms is supposed to be established quickly, and both oxides are supposed to be completely in the ionized state:

$$K_2O \Leftrightarrow 2K^+ + O^{2-},\ K_{eq} = \infty,\quad p[O^{2-}]_{eq} = p[K_2O]_0 \qquad \text{(R25)}$$

$$Na_2O \Leftrightarrow 2Na^+ + O^{2-},\ K_{eq} = \infty,\ p[O^{2-}]_{eq} = p[Na_2O]_0 \qquad \text{(R26)}$$

Therefore, in the hot corrosion literature, there is a variety of ways of expressing the melt basicity either as $p[O^{2-}]$ or $p[Na_2O]$ or $p[K_2O]$. All these markings reflect the $[O^{2-}]$ concentration in the melt, and usually all mean $p[O^{2-}]$, but they are not exactly the same if analysed in detail. This way of determining the basicity is also different than in aqueous solutions, where the acid–base scale is determined from the auto-ionization of H_2O molecules with the assumption that the solutions are dilute, and therefore activity of H_2O can be assumed to be 1:

$$H_2O \Leftrightarrow OH^- + H^+,\ K_{eq} = 10^{-14},\ p[H^+] + p[OH^-] = 14 \quad \text{(at 25 °C)} \qquad \text{(R27)}$$

Because molten salt electrolytes are not dilute solutions, one cannot assume a certain component to always form the solvent phase of the ionic solution, like in water solutions. This is an important difference of how the basicity scale is

determined in molten salt chemistry versus aqueous solution chemistry. Furthermore, because the basicity scale is determined from the activity of the O^{2-} ion only, the scale itself is somewhat ambiguous. In simple salts, the counter cation with which the O^{2-} ion is equilibrated may be known exactly, but in complex salts, the O^{2-} ion may be equilibrated with several cations (e.g. the Na_2O-K_2O-CaO system). Furthermore, the formation of peroxide (O_2^{2-}) and superoxide ions (O_2^{-}) in some salt systems changes the O^{2-} ion equilibrium in the melt and makes the estimation of the [O^{2-}] concentration simply from the K_2O or Na_2O formation equilibrium inaccurate, and should instead be measured directly by solid-state selective ion reference electrodes (such as Y_2O_3 doped ZrO_2 for O^{2-} ion). In practical applications, the corrosive molten salt system may be very complicated, and the most active corrosive ion is not necessarily the O^{2-} ion at all, even though the corrosion or dissolution rates are presented as a function of p[O^{2-}]. However, the dissolution rates are still modified by the changes in the basicity of the melt, and therefore, for engineering purposes, it is a convenient way to compile and present the corrosion data.

5.4.3 Corrosion under molten Na_2SO_4

Hot corrosion by molten Na_2SO_4 is the most well studied hot corrosion system due to its importance in gas turbine corrosion. Gas turbines operated in the vicinity of sea water were found to have formed white deposits on the turbine blades and vanes and experienced catastrophic corrosion rates. The white deposit was analysed and turned out to be Na_2SO_4. Later research revealed the corrosion to be caused by a thin liquid Na_2SO_4(l) layer that formed on the component surface. Under molten Na_2SO_4, the corrosion reaction may follow either basic or acidic dissolution. For example, in case of the NiO-forming alloy:

Basicity scale: $Na_2SO_4 \Leftrightarrow Na_2O + SO_3(g)$, (R28)

$p[Na_2O] + p[SO_3(g)] = 17.4$ (at 900 °C)

Basic dissolution: $2NiO + Na_2O + ½O_2(g) \Leftrightarrow 2NaNiO_2$ (R29)

Acidic dissolution: $NiO + Na_2SO_4 \Leftrightarrow NiSO_4 + Na_2O$ (R30)

Similar reactions can be suggested for other oxides, as well. Figure 13 compiles the data for various protective oxides.

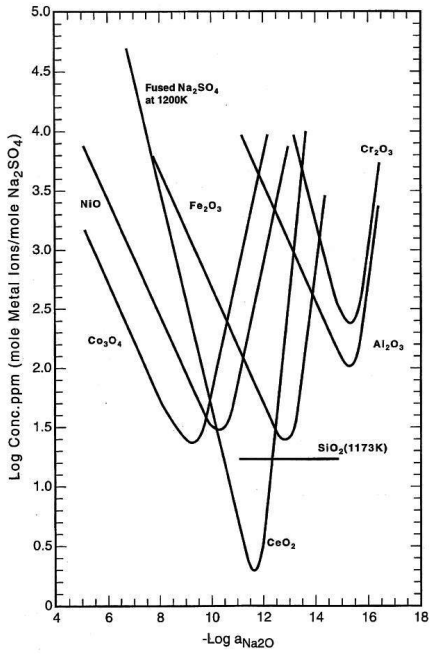

Figure 13. Dissolution of protective oxides in molten sodium sulphate as a function of melt basicity (Rapp, 2002) with permission from Elsevier.

5.4.4 Corrosion under molten K_2SO_4

There has not been much work on corrosion under pure K_2SO_4 salt. It is assumed to corrode metals very similarly to an Na_2SO_4 melt. However, in biomass combustion, potassium is the major alkali instead of sodium, which is typically the major alkali in coal combustion. Adding K_2SO_4 to the Na_2SO_4 salt tests generally increases the corrosion rates compared to pure Na_2SO_4. This can be attributed to the lowering of the melting point of the salt mixture compared to the pure salts (Shi, Zhang, & Shih, 1992).

5.4.5 Corrosion under molten KCl

Most work concerning corrosion in biomass-fired systems has focused on the effect of KCl(s,l,g) on the corrosion of superheaters. Alkali deposits on superheaters in biomass-fired boilers contain mostly KCl(s,l) and K_2SO_4(s,l) as the deposit-forming compounds. These compounds are even more abundant in the inner parts of the deposits in contact with the tube material. Therefore, it has generally been assumed that either KCl(s,l) or K_2SO_4(s,l) are the compounds that initially condense on the superheater tubes and form the initial condensation layer (Montgomery, Karlsson, & Larsen, 2002; Broström, Enestam, Backman, & Mäkelä, 2013; Hansen, Jensen, Frandsen, Sander, & Glarborg, 2017; Damoe, Jensen, Frandsen, Wu, & Glarborg, 2017). Because of the very low saturation vapour pressure of K_2SO_4(s,l) (~0.3 Pa at 1000 °C), it has been assumed that most of the K_2SO_4(g) in gas phase should form aerosols or condense on the larger ash particles before the superheater area. Therefore, KCl(g) condensation is generally assumed to be the main mechanism for

the initial condensation layer formation, and the K_2SO_4(s,l) found in the mature deposits is formed by the heterogeneous reaction of the KCl(s,l) with SO_2(g)/SO_3(g) in the flue gases forming the KCl-K_2SO_4 mixture. During the heterogeneous sulphation of KCl(s,l), Cl_2(g) or HCl(g) gas is assumed to form, which then could attack the tube material with a gas-phase chlorine mechanism (section 5.3). In addition to gas-phase chlorine attack, it has been suggested that the KCl(s)-containing deposit layer may become molten when the metal chlorides ($FeCl_2$(s,l,g) $CrCl_2$(s,l,g), $FeCl_3$(s,l,g), $CrCl_3$(s,l,g)) formed in the gas-phase chlorine attack form a eutectic mixture with it (Montgomery, Carlsen, Biede, & Larsen, 2002). Even without the metal chlorides, it has been suggested that a local eutectic mixture may form in the KCl-K_2SO_4 system or in the KCl-K_2SO_4-NaCl-Na_2SO_4 system, because the superheater deposits always also contain at least trace amounts of sodium. Hot corrosion rates under molten chlorides are typically higher, or as high as hot corrosion rates under molten sulphates, but because of the generally lower melting points of chlorine-containing deposits, the very high corrosion rates are encountered at already lower service temperatures. Figure 14 presents a compilation of dissolution rates of protective oxides in molten chloride-containing alkali mixtures.

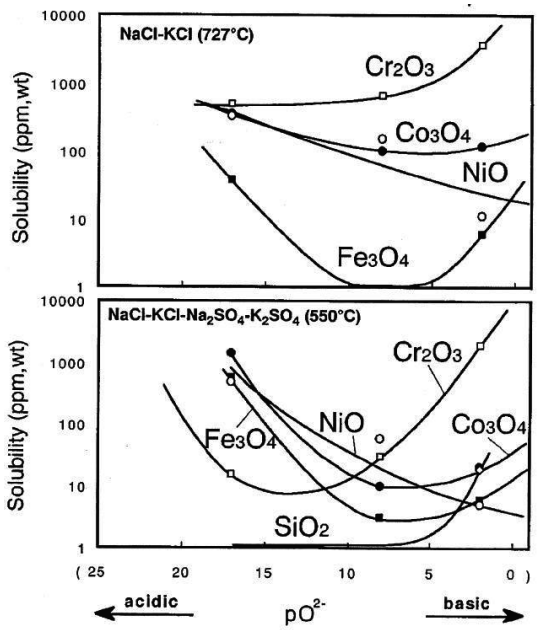

Figure 14. Dissolution of protective oxides in molten alkali chloride salts as a function of melt basicity (Ishitsuka & Nose, 2000). Reprinted from Materials and Corrosion, Copyright (2000) Wiley-VCH Verlag GmbH & Co. KGaA. Reproduced with permission.

5.4.6 Corrosion under molten K_2CO_3

Corrosion in molten carbonate salts has been studied quite a great deal, because of their importance in molten salt fuel cells. The corrosion of electrode materials in these devices is a major problem that needs to be solved before large-scale commercial adaptation of this technology is possible (Hsu, DeVan, & Howell, 1987;

Ota, et al., 1995; Lee & Shores, 1990; Giddey, Badwal, Kulkarni, & Munnings, 2012). Although similar, the service conditions are not exactly the same as in hot corrosion. In the fuel cells, the corrosion is happening in a deep melt with essentially constant electrolyte composition, whereas in hot corrosion, the molten salt layer is so thin that the gas phase surrounding the metal surface is rapidly interacting with the melt when the gases diffuse through the molten layer or dissolve in the melt, changing its basicity and composition. The operation temperature of the fuel cell is around 600 °C. Ni-Al or Ni-Cr alloys are used as anode materials, NiO as the cathode material and and Li_2CO_3/K_2CO_3 mixture as the electrolyte (Vossen, Plomp, de Wit, & Rietveld, 1995; Antolini, 2011). The electrolyte is suspended in a $LiAlO_2$ matrix. The basicity of the melt in the fuel cell is determined by the equilibrium:

$K_2CO_3 \Leftrightarrow K_2O + CO_2(g)$ $\quad p[K_2O] + p[CO_2(g)] = 15.8$ (at 600 °C) (R31)

The fuel cell reaction at the cathode is:

$CO_2(g) + ½O_2 + 2e^- \Leftrightarrow CO_3^{2-}$ (R32)

and at the anode:

$CO_3^{2-} + H_2 \Leftrightarrow H_2O(g) + CO_2(g) + 2e^-$ (R33)

The cathode is susceptible to acidic dissolution:

$NiO + CO_3^{2-} \Leftrightarrow NiCO_3 + O^{2-}$ (R34)

and the anode to the precipitation of the dissolved Ni:

$Ni^{2+} + 2e^- \Leftrightarrow Ni$ (R35)

Precipitation of Ni in the electrolyte leads eventually to short-circuiting the cell membrane and malfunctioning of the cell. The dissolution rate of the cathode material is the lifetime-limiting factor in molten carbonate fuel cells. One way to increase the lifetime of the cathode material is by keeping the basicity of electrolyte at the dissolution minima of NiO, analogous to the NiO dissolution minima in molten Na_2SO_4 at $p[O^{2-}] \approx 10.5$, as shown in Figure 13.

5.4.7 Corrosion under molten KOH

Corrosion studies of constructional materials under molten KOH or NaOH have been done in the past because of their potential use as the heat transfer fluid in molten salt-cooled nuclear reactors (Smith, 1956). Some earlier hot corrosion studies in combustion gases have also been done, because alkali hydroxides were proposed as ionizing additives in coal-fired magnetohydrodynamic (MHD) generators (Aref´´ev, Ivashchenko, Suslova, & Khomchenkov, 1969). More recently, direct carbon molten hydroxide fuel cells have been investigated (Giddey, Badwal, Kulkarni, & Munnings, 2012; Guo, Calo, DiCocco, & Bain, 2013). These earlier studies have concluded that the majority of steel grades and nickel alloys are unsuitable construction materials for molten hydroxide fluids (Nickel Institute,

1973). The best corrosion resistance in molten hydroxide is for pure Ni, because of the stability of NiO in basic alkali melts. In molten KOH, the overall corrosion reactions for Ni can be explained as follows (Tzvetkoff & Gencheva, 2003; Tzvetkoff & Girginov, 1995; Bozzini, et al., 2012; Tran, Mao, & Barham, 1992):

Basicity scale: $2KOH \Leftrightarrow K_2O + H_2O(g)$, (R36)

$p[K_2O] + p[H_2O(g)] \Leftrightarrow 11.3$ (at 500 °C)

Basic dissolution: $2NiO + K_2O + ½\ O_2(g) \Leftrightarrow 2KNiO_2$ (R37)

Acidic dissolution: $NiO + 2KOH \Leftrightarrow Ni(OH)_2 + K_2O$ (R38)

However, sulphur or chlorine impurities in the hydroxide melts increase the corrosion rate of Ni substantially. Therefore, in the case of biomass combustion flue gases, if a molten alkali hydroxide layer is formed on the superheater tubes, it will be contaminated with sulphur and chlorine, and even the most expensive Ni-based alloys can show high corrosion rate.

5.4.8 Complexity of molten salt chemistry in actual service conditions

A major challenge for hot corrosion studies in boilers is to duplicate the chemistry of the actual service conditions in the laboratory tests. The fouling and corrosion reactions in biomass-fired boilers definitely involve alkali metals, sulphur and chlorine (all cases). In some cases, this fouling and corrosion involve phosphorus (bone meal, municipal sludge), heavy metals (waste biomass from construction sites, municipal solid waste) and possibly fluorine or bromine (waste biomass from construction sites or hospital waste). Therefore, the chemical environment that can form on the superheater surfaces may be complicated. With detailed ex-situ analysis of the deposits using the current analysis techniques available, practically any element can be found at least in trace amounts in the deposits. Because the corrosion reactions with the alloy depend on the detailed chemistry of the melt, even the trace amounts can change the corrosion rates in hot corrosion conditions substantially. Therefore, recently, on-line techniques have been developed trying to measure the corrosion rates in the boilers with electrochemical methods, such as galvanic pair activity, the linear polarization (LPR) method, electrochemical impedance spectroscopy (EIS) and electrochemical noise (EN) (Retschitzegger, Brunner, Obernberger, & Waldmann, 2013; Retschitzegger, Gruber, Brunner, & Obernberger, 2015; Gruber, Schulze, Scharler, & Obernberger, 2015). While the on-line electrochemical probes respond quickly to the dynamics of corrosion reactions in the boilers, the chemical interpretations of the results is difficult. The electrochemical signal must be correlated with mass loss coupon data to validate the corrosion rate results. Detailed chemistry correlations of the reactions happening at the electrodes with the electrochemical output signal do not exist and may be impossible to achieve. However, the value of these methods lies in their fast response times and capability to estimate the relative corrosion rate changes – for example, when the fuel mixture in the boiler is changed. It is very likely that the biomass power plants need to be able to combust different types of biomass available near the plant. Electrochemical on-line estimations of the corrosion rates enables the plant operators to optimize the process conditions in the combustors in real-time in order to minimize the corrosion damage to the boiler.

6. Experimental methods

6.1 Molar balance calculations

Mass and molar balance calculations are the very basic methodology used in combustion science and in reaction engineering in general. They are based on the conservation of mass. The mass flow of an element that goes into the furnace must come out in some compound or accumulate in the furnace. The elemental composition of the fuel and its mass flow rate are used as the inputs. The output is the flue gas and ash flow rates. In order to construct the output flows, some assumptions of the compounds they contain are needed. The major fuel elements – carbon, hydrogen, sulphur and nitrogen – are assumed to react to $CO_2(g)$, $H_2O(g)$, $SO_2(g)$ and $N_2(g)$. Then, the oxygen content needed for the stoichiometric oxidation is calculated, and the oxygen content of the fuel is subtracted from this value. If combustion happens in air, the diluting nitrogen content is calculated from the required oxygen content and added to the output $N_2(g)$.

For the ash-forming elements, the elemental input flow is determined from the elemental analysis of the ash and the ash content. The fuel sample is ashed, and the elemental analysis of the residual ash is measured with XRF. The input mass flow of each element is estimated by the weight-% of that element in the ash, multiplied by the ash content of the fuel in weight-%, multiplied by the fuel mass flow. When calculating the weight-% of the elements is the ash, the chemical forms of the compounds in the ash are assumed to be the oxides of the elements. This assumption is not actually correct for all the ash-forming elements, especially for potassium, sodium and calcium. These elements are actually found as sulphates, chlorides or carbonates in the output flows. Furthermore, the ash content of some biomass-based fuels can be very low (<1 w-%), and some volatile ash-forming elements can be vaporized during the ashing procedure (1 hour at 815 °C in air if coal standard is used). Therefore, the standard analysis technique is not very accurate for the determination of K, Na and Ca contents in the fuel. More accurate results for these compounds can be achieved if the analysis is conducted directly from the fuel sample, by leaching the fuel sample with $H_2O/CH_3COONH_4(aq)/HCl(aq)$ and then analysing these elements from the leachates. This chemical fractionation method gives additional information on the release patterns of these elements during combustion, as the part leached in the less aggressive solvents (H_2O/CH_3COONH_4) is released to the gas phase more readily than the part that is only leached in HCl (Werkelin, Skrifvars, Zevenhoven, Holmblom, & Hupa, 2010).

Based on the knowledge of the behaviour of the ash-forming elements in the boiler (especially K, Na, Ca, S and Cl), fuel indices aimed at predicting the fouling and corrosion risk of the fuel can be calculated from the abundance of the ash-forming elements in the fuel. The fuel indices can be calculated on a mass or molar basis, or by using the heat value of the fuel on an energy basis. With biomass-based fuels, it is popular to calculate the indices on a molar basis, whereas in the older coal combustion literature, the indices are normally calculated on a mass or energy basis. The use of the molar basis in biomass combustion is reasonable, because of the chemical insight it gives into the behaviour of K, Na, Ca, S and Cl.

6.2 Multicomponent thermodynamic calculations

Multicomponent thermodynamic calculations are based on the minimization of the Gibbs free energy of the system (Roine, 2014). It is, in principle, a more sophisticated mass balance of the reacting system. In basic stoichiometric calculations, the output compounds are fixed using empirical knowledge of the output composition, whereas in multicomponent thermodynamic calculations, the most likely output composition is calculated from the thermodynamic properties of the compounds. The standard Gibbs free energy (298 K, 100 kPa) of formation of an individual component is:

$$\Delta G_f^0 = \Delta H_f^0 - T\Delta S_f^0 \quad (3)$$

At other than NTP conditions, the Gibbs free energy of the reaction is:

$$\Delta G_f = \Delta H_f^0 + \int_{298}^{T} \Delta C_p dT - \left(T\Delta S_f^0 + \int_{298}^{T} \frac{\Delta C_p}{T} dT - Rln\left(\frac{P}{100kPa}\right)\right) \quad (4)$$

which gives the temperature and pressure dependence (pressure term is neglected for solids and liquids) of the Gibbs free energy of the reaction. Heat capacities as a function of temperature are obtained by fitting polynomial functions to the measured heat capacities. The measured values for different compounds are stored in databanks or books, such as the JANAF tables. In the case of multicomponent systems, the total Gibbs free energy of the system is calculated by summation of the contributions of all the pure components, plus the excess Gibbs free energy:

$$G_f^{total} = \sum_i^N n_i \mu_i + \Delta G_{mix} \quad (5)$$

where μ_i is the chemical potential of the pure compound (Gibbs energy per mole of the component, G/n); n_i is the mole number of the component; and N is the number of components. The first term of this equation can be evaluated using the tabulated thermodynamic data. The second term takes into account the changes in the chemical potentials of the individual components when they are in the mixture. There are many ways evaluating the second term, and the most suitable method depends on the type of the mixture phase (solid solution, aqueous solution, molten salt, gas mixture, etc.). The algorithm in the Gibbs energy minimization software then attempts to minimize the total Gibbs free energy of the whole system by varying the amounts of the individual components in the system with the constraint that the elemental balance between the input and output system is conserved. The result is an energetically optimal composition for the system at a given temperature and pressure (Figure 15).

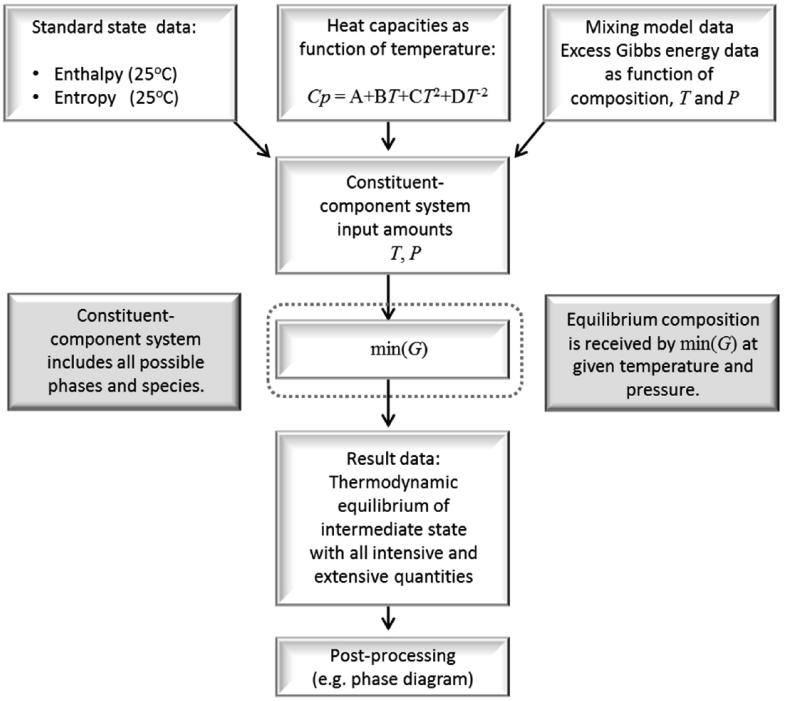

Figure 15. Schematic of the general calculation flow in Gibbs energy minimization software packages (Koukkari, 2014). Reproduced with permission.

6.2.1 Kinetic limitations

Equilibrium calculations provide a good starting point when estimating the most likely compositions of the flue gases and deposits formed in the boiler. Due to the high temperatures in the furnace section of a boiler, it is generally a good approximation that kinetic limitations are not important there. However, after the flue gases have escaped from the furnace, they experience rather high cooling rates. Therefore, in the post-combustion gases, a certain kinetic limitation may become important. Concerning alkali transformations, the most studied one is the sulphation of KCl(s,l,g) in the flue gases. Several papers have suggested that the gas phase sulphation is kinetically controlled at typical furnace exit gas temperatures (Mortensen, Hashemi, Wu, & Glarborg, 2019; Jiménez & Ballester, 2005; Nielsen, et al., 2000). It has also been suggested that nucleation of the gas phase K_2SO_4(g) to K_2SO_4(s) aerosols is kinetically limited in the flue gases. In the case of fluidized bed boilers, the agglomeration of the bed material is definitely kinetically controlled. Bed material agglomeration involves reactions of SiO_2(s) with KOH(l,g) or KCl(l,g). Because SiO_2 is solid at the typical CFB furnace temperatures and because of the rather low combustion temperatures in CFB boilers (~ 850 °C), this gas–solid or liquid–solid reaction has been shown to be kinetically controlled at these process conditions (Anicic, Lin, Kim, & Wu, 2018). Kinetic limitation are not able to be included in the basic Gibbs energy minimization calculations, however, recently developed methods make it possible to use kinetic constraints for particular reactions in the system, while the rest of the system is assumed to reach thermodynamic equilibrium.

6.2.3 Mass transfer limitations (mixing)

Thermodynamic equilibrium calculations assume a perfectly mixed reacting system. Real-life boilers cannot be considered as perfectly mixed reactors. The combustion gases and ash products are not evenly distributed in the boiler, but generally form a distinctive flow pattern in the boiler. This makes it possible for local chemical environments in the boiler to exist that differ from the thermodynamically predicted chemical environment calculated from the fuel's elemental composition. There are, for example, regions of high and low oxygen activity in the furnace where the combustion air is mixed with the fuel. These differences are not generally taken into account in the thermodynamic equilibrium calculations, but can be studied by a combination of computational flow dynamic (CFD) simulations with equilibrium calculations. CFD calculations can be used to estimate the local elemental amounts of the input system for the Gibbs energy minimization, and then a local chemical equilibrium can be calculated (Mueller, Skrifvars, Backman, & Hupa, 2007). The method is computationally exhaustive, but can provide a three dimensional chemistry map in the boiler, thus better simulating the risky areas where, for example, extensive deposit formation can be expected.

6.3 XRD analysis

X-ray diffraction (XRD) analysis is a powerful analytical technique to identify unknown crystalline compounds in the sample. It is based on the constructive and destructive interference of X-rays when diffracted from the atoms in the crystal. The detailed rules in the diffraction of X-rays from crystals are complicated and calculated with dynamic X-ray diffraction theory. Each lattice plain in a crystal constitutes a unique composition and ordering of atoms within the plane. In certain conditions, known as Bragg conditions, diffraction of X-rays in the lattice plane form an interference pattern that can be formulated as if the plane reflects the incoming X-rays:

$$2dsin\theta = n\lambda \tag{6}$$

where d = spacing between the lattice planes
θ = incident angle of the X-rays
n = integer
λ = wavelength of the X-rays

This is seen as intensity peaks in the diffracted X-rays as a function of the incident angle between the X-rays and the lattice plane. Each compound has its characteristic crystal structure and atomic plane distances within. In a randomly oriented polycrystalline sample (powder diffraction), all the lattice planes present in the crystal reach the Bragg condition at some incident angle θ and an intensity peak is detected in the diffracted x-ray detector at 2θ. The sample is scanned over a range of θ angles, and a 2θ-intensity pattern is produced. Comparing the measured peaks to the peaks in a library of known compounds, the compounds can be identified.

6.4 UV/VIS spectroscopy

Absorption spectroscopy in the visible or ultraviolet range of electromagnetic radiation is used as a standard laboratory method to quantify the concentrations of ions and molecules in a solution. Visible and UV ranges in the spectrum correspond to energies in the electron transitions between the molecular orbitals in the compounds. Molecules dissolved in water have broader absorption peaks than the molecules in the gas phase due to the intermolecular effects between the water molecules and the analyte molecules in the solution. The intermolecular effects blur the quantized nature of the electron transfer energies, which makes absorption peaks appear like continuous absorption spectra. Light absorption is proportional to the concentration of the molecule in the solution according to the Beer–Lambert law:

$$-log\left(\frac{I}{I_0}\right) = A = \varepsilon bc \tag{7}$$

where I_0 = intensity of the light beam without the sample
I = intensity of the light beam with the sample
A = absorbance
ε = molar absorptivity of the molecule
b = thickness of the sample
c = concentration of the molecule in the sample

In practice, the analysis is done by preparing a series of standard solutions with known concentrations of the molecule and then preparing the standard curve for the absorbance-concentration relation. The concentration of the molecule in the sample is then estimated by calculating the concentration using the standard curve.

6.5 Galvanic cell probe

In Publication 1, a high temperature electrochemical probe was used. The probe is based on the principle of galvanic cells. Different materials have different electrochemical activity when immersed in an ionic liquid. Normally, the ionic electrolyte is a water solution, but molten salts also act as ionic electrolytes. Even solids can function as ionic conductors at high temperatures. For example, the commonly known lambda sensor is based on the ionic conductivity of O^{2-} ions in solid ZrO_2 at high temperatures. The electromotive force (voltage) of the galvanic couple is given by the Nernst equation:

$$E_{cell} = E^0_{cell} - \frac{RT}{zF} ln \frac{\prod_j a_j^{\nu_j}}{\prod_i a_i^{\nu_i}} \tag{8}$$

where E^0_{cell} = cell potential in standard conditions
R = gas constants
T = temperature
z = number of electrons transferred in the cell reaction
F = Faraday's constant
a_j = activity of individual component in the products of reaction
ν_j = stoichiometric coefficient of the individual component in the products of reaction

a_i = activity of individual component in the reactants of reaction
ν_i = stoichiometric coefficient of the individual component in the reactants of reaction

The current through the galvanic cell is given by the Faraday's law, which relates the galvanic cell current to the corrosion rate:

$$q = Idt = zFdn \quad (9)$$

$$I = zF\frac{dn}{dt} \quad (10)$$

where q = charge
z = number of electrons transferred in the cell reaction
F = Faraday's constant
$\frac{dn}{dt}$ = molar flow rate of ions

Aqueous solutions have long been studied, and standard cell potentials relative to the hydrogen electrode have been determined for a number of known electrode reactions. The problem when using this technique to measure electrochemical activity of the deposits in boilers is that the composition of the electrolyte and the reactions happening at the electrodes are unknown. Therefore, the voltage measured does not give any chemical information on the system. For the same reason, the current measured does not relate to real mass loss, because the number of electrons transferred in the cell reaction are not known. However, the probe signal still measures the electrochemical activity at the electrode-electrolyte interface. When varying the surface temperature of the probe by cooling the air flow rate, this electrochemical activity can be measured as a function of probe surface temperature. The point at which the voltage and current signals start deviating from zero is the onset temperature at which the electrochemical activity starts. Based on this onset temperature, an interpretation was made that at this point, the deposit became ionically conductive and likely molten.

7. Main findings of the research

The following sections present the main findings of our research. The results are only briefly discussed, and for the more detailed results, the reader is encouraged to study the publications referred to (attached at the end of the printed version of this thesis).

7.1 Effect of the molar balance of K, Na, S and Cl on the thermodynamically stable potassium species

The alkali, sulphur and chlorine chemistry in the gas phase is highly coupled, as shown in R1-R6. Therefore, if mass transfer limitations (because of non-perfect mixing) and kinetic limitations in the reactions are omitted, the mole fractions of these elements in the gas phase can be used to estimate the amounts of alkali sulphates, chlorides and hydroxides/carbonates formed. In all of the publications,

this methodology was used to estimate the amount of KOH(g)/K_2CO_3(g) or K(g)/Cl(g) molar ratio in the flue gases. During the process of this research, the following equations were developed:

$$[KOH(g)]_{(energy\ basis)} \sim \frac{[K_{sol}]+[Na_{sol}]-2[S]-[Cl]}{LHV} \quad (11)$$

$$[KOH(g)+KCl(g)]_{(energy\ basis)} \sim \frac{x([K]+[Na])-2[S]}{LHV} \quad (12)$$

$$[KOH(g)]_{(molar\ basis)} \sim x([K]+[Na])-2[S]-[Cl] \quad (13)$$

$$\frac{[K(g)]}{[Cl(g)]}(molar\ ratio) \sim \frac{x([K]+[Na])-2[S]}{[Cl]} \quad (14)$$

where $[K_{sol}]$ = acetic acid soluble fraction of the potassium in the fuel, mol/kg fuel
$[Na_{sol}]$ = acetic acid soluble fraction of the sodium in the fuel, mol/kg fuel
x = conversion of fuel alkali to vaporized alkali
[K] = potassium content of the fuel, mol/kg fuel, dry basis
[Na] = sodium content of the fuel, mol/kg fuel, dry basis
[S] = sulphur content of the fuel, mol/kg fuel, dry basis
[Cl] = chlorine content of the fuel, mol/kg fuel, dry basis
LHV = lower heating value of the fuel, MJ/kg fuel

The underlying principle in these equations is the conservation of the elemental balance between the input fuel and the output ash and flue gases. The estimation of the relative amount of alkali vaporized in the gas phase (conversion) is estimated either by assuming that the acetic-acid-soluble fraction of these elements in the fuel represents the fraction that is released to the gas phase during combustion, or with an adjustable parameter (x). Using an adjustable parameter is convenient for modelling, because one can estimate different situations even without knowing the actual conversion values in particular process conditions.

These simple equations also contain information about the thermodynamics of the alkali chemistry in the gas phase (R1-R6): alkali sulphates are formed first, and then, when all sulphur has been consumed by the alkali reactions, alkali chlorides start forming, and when all sulphur and chlorine have been consumed, alkali carbonates and hydroxides start forming. The molar sulphur content of the fuel is multiplied by 2 because one mole of sulphur consumes two moles of alkali when forming alkali sulphates. The approximation that these equations represents the concentration of KOH(g) in the flue gases is based on two assumptions:

1. The sodium content of biomass fuels is normally very low, and therefore [Na] can be set to zero in most cases.

2. K_2CO_3(g) is not stable in the gas phase until very low gas temperatures are reached, and therefore it can be neglected as the gas-phase, alkali-bearing species.

Equations (11)-(14) were used to study a number of different biomass and fossil fuels, as shown in Tables 2 and 3, and some very interesting observations were made. First of all, it became clear that calculating these parameters for fossil fuels led to negative values, and positive values resulted for biomass-based fuels. The physical interpretation is that fossil fuels have so much more sulphur than alkali that all the fuel alkali can react to alkali sulphates, and there is still surplus sulphur left in the fuel. This excess sulphur forms $SO_2(g)/SO_3(g)$ in the flue gases during combustion. Secondly, a clear trend was found with equation (13) for biomass-based fuels. Namely, the agricultural-based fuels resulted in orders of magnitude larger KOH(g) values than forest-based biomass fuels. This result is consistent with the empirical knowledge that agricultural residues and other short-rotation coppices are generally more problematic than stem wood from the fouling and corrosion point of view. Lastly, equation (14) led to the observation that the K(g)/Cl(g) molar ratio is largest for stem wood. This result suggests that while the relative amount of KOH(g) over KCl(g) in the flue gases may be higher in forest-based, biomass-fired units, the absolute amount of KOH(g) in the flue gases may be important in both cases.

Table 2. Fuels sorted with equation (13).

Fuel	[K], dry basis	[Na], dry basis	[Cl], dry basis	[S], dry basis	[K], in ash	[Si], in ash	[Si]/[K]	[KOH(g)] x=0	[KOH(g)] x=0.2	[KOH(g)] x=0.4	[KOH(g)] x=0.5	[KOH(g)] x=0.6	[KOH(g)] x=0.8	[KOH(g)] x=1
	mg	mg	mg	mg	g	g		mmol	mmol	mmol	mmol	mmol	mmol	mmol
	kg fuel	kg fuel	kg fuel	kg fuel	kg ash	kg ash		kg fuel	kg fuel	kg fuel	kg fuel	kg fuel	kg fuel	kg fuel
Brasica Carinata straw	15414	0	600	2800	400.0	25.0	0.1	-191.4	-112.6	-33.7	5.7	45.1	123.9	202.8
Wheat straw	10910	230	2890	800	168.0	272.0	1.6	-131.4	-73.6	-15.8	13.1	42.0	99.8	157.6
Maize straw	11776	0	6400	700	220.0	330.0	1.5	-224.2	-163.9	-103.7	-73.6	-43.5	16.8	77.0
Wheat Marius straw	7263	0	2700	600	170.0	640.0	3.8	-113.6	-76.4	-39.3	-20.7	-2.1	35.0	72.2
Rape straw	4623	0	300	1000	120.0	90.0	0.8	-70.8	-47.1	-23.5	-11.7	0.2	23.8	47.4
Forest residue	2110	110	240	400	72.0	120.0	1.7	-31.7	-20.0	-8.2	-2.3	3.5	15.3	27.0
Bark (pine)	1120	50	110	300	63.0	6.0	0.1	-21.8	-15.6	-9.5	-6.4	-3.3	2.9	9.0
Sawdust (pine)	500	40	15	100	102.0	39.0	0.4	-6.7	-3.8	-0.8	0.6	2.1	5.0	7.9
Peat, surface	690	380	180	1000	24.0	245.0	10.2	-67.4	-60.6	-53.7	-50.3	-46.9	-40.1	-33.2
Peat, carex	440	330	270	2000	11.0	201.0	18.3	-132.3	-127.1	-122.0	-119.5	-116.9	-111.8	-106.7
Rhein brown coal	140	300	250	3000	3.0	64.0	21.3	-194.0	-190.7	-187.4	-185.7	-184.0	-180.7	-177.4
Iowan Rawhide coal	570	1140	25	5000	6.0	162.0	27.0	-312.3	-299.5	-286.7	-280.2	-273.8	-261.0	-248.2
Polish bituminous coal	1420	450	760	7000	14.0	198.0	14.1	-457.7	-446.5	-435.4	-429.8	-424.2	-413.0	-401.8
Columbian bituminous coal	2600	440	130	10000	15.0	280.0	18.7	-626.9	-609.8	-592.7	-584.1	-575.5	-558.4	-541.3
Illinois no 6, bituminous coal	3610	1420	1210	29000	23.0	250.0	10.9	-1841.5	-1810.7	-1779.9	-1764.5	-1749.1	-1718.3	-1687.5

Table 3. Fuels sorted with equation (14).

Fuel	K, ppm	Na, ppm	Cl, ppm	S, ppm	K, % in ash	Si, % in ash	Si/K	K(g)/Cl(g) x=0	K(g)/Cl(g) x=0.2	K(g)/Cl(g) x=0.4	K(g)/Cl(g) x=0.5	K(g)/Cl(g) x=0.6	K(g)/Cl(g) x=0.8	K(g)/Cl(g) x=1
Sawdust (pine)	500	40	15	100	10.2	3.9	0.4	-14.7	-7.9	-1.0	2.4	5.9	12.7	19.6
Brasica Carinata straw	15414	0	600	2800	40.0	2.5	0.1	-10.3	-5.7	-1.0	1.3	3.7	8.3	13.0
Rape straw	4623	0	300	1000	12.0	9.0	0.8	-7.4	-4.6	-1.8	-0.4	1.0	3.8	6.6
Forest residue	2110	110	240	400	7.2	12.0	1.7	-3.7	-2.0	-0.2	0.7	1.5	3.3	5.0
Bark (pine)	1120	50	110	300	6.3	0.6	0.1	-6.0	-4.0	-2.1	-1.1	-0.1	1.9	3.9
Wheat straw	10910	230	2890	800	16.8	27.2	1.6	-0.6	0.1	0.8	1.2	1.5	2.2	2.9
Wheat Marius straw	7263	0	2700	600	17.0	64.0	3.8	-0.5	0.0	0.5	0.7	1.0	1.5	1.9
Maize straw	11776	0	6400	700	22.0	33.0	1.5	-0.2	0.1	0.4	0.6	0.8	1.1	1.4
Peat, surface	690	380	180	1000	2.4	24.5	10.2	-12.3	-10.9	-9.6	-8.9	-8.2	-6.9	-5.6
Peat, carex	440	330	270	2000	1.1	20.1	18.3	-16.4	-15.7	-15.0	-14.7	-14.4	-13.7	-13.0
Polish bituminous coal	1420	450	760	7000	1.4	19.8	14.1	-20.4	-19.8	-19.3	-19.1	-18.8	-18.3	-17.8
Rhein brown coal	140	300	250	3000	0.3	6.4	21.3	-26.5	-26.1	-25.6	-25.4	-25.1	-24.7	-24.2
Illinois no 6, bituminous coal	3610	1420	1210	29000	2.3	25.0	10.9	-53.0	-52.1	-51.2	-50.7	-50.3	-49.4	-48.5
Columbian bituminous coal	2600	440	130	10000	1.5	28.0	18.7	-170.1	-165.4	-160.8	-158.4	-156.1	-151.4	-146.8
Iowan Rawhide coal	570	1140	25	5000	0.6	16.2	27.0	-442.3	-424.1	-405.9	-396.8	-387.7	-369.5	-351.3

7.2 In-situ galvanic probe measurements

In Publication I, the galvanic probe was used to measure the electrochemical signal of the deposit on-line. The measurements were done in a large-scale CFB unit burning forest residue as the fuel. The voltage and current signals started to show increased activity around 400 °C metal temperature, which indicated a possible melting point of the deposit at this temperature. This observation was consistent with the KOH(g) → KOH(l) condensation mechanism presented in detail in the theoretical work in Publications II and III. In these publications, it was argued with the aid of equations (11) and (14) and thermodynamic calculations that in general, biomass-based fuels tend to contain much more available potassium than chlorine, even if one assumes that the fuel sulphur first reacts completely to $K_2SO_4(s)$. Because the estimated [K(g)]/[Cl(g)] molar ratios were found to be higher than 1, it was suggested that this indicates the existence of KOH(g) in the gas phase in the convection superheater area of a boiler. The formation of $K_2CO_3(s)$ likely follows a heterogeneous route, forming in the heterogeneous reaction of $CO_2(g)$ with the condensed KOH(l). This mechanism would explain the existence of KOH(l) on the superheater tube surfaces and thus its involvement in the corrosion reactions with the alloys.

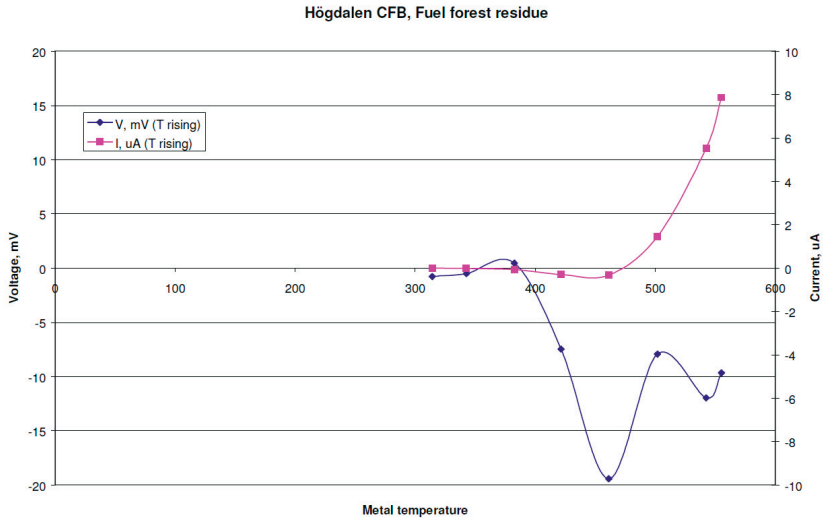

Figure 16. Galvanic probe signal as a function of probe temperature. (From Publication I) with permission from Trans Tech Publications Ltd.

7.3 Correlation of corrosion rates in biomass boiler with KOH(g)-K_2CO_3(g) equilibrium

In Publication IV, an extremely interesting and important observation was made. It was found that the thermodynamically predicted amount of KOH(g) in flue gases correlated very nicely with the reported corrosion rates in a full-scale, straw-fired boiler as a function of temperature, as shown in Figure 17. This observation provides further evidence that the partial pressure of KOH(g) in the flue gases may play a more important role in the fouling and corrosion processes than has previously been thought. The fact that the partial pressure of KOH(g) could be estimated from the chemical analysis with equation (13) provides the necessary

connection to the fuel properties needed for the practical significance of the work.

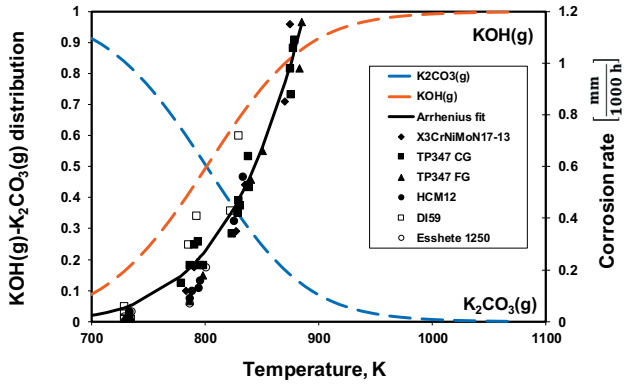

Figure 17. Thermodynamically predicted KOH(g)-K_2CO_3(g) equilibrium superimposed on the graph of corrosion rates of different steel grades in a straw-fired boiler as a function of metal temperature. From Publication IV, with permission from Elsevier.

7.4 Reactions in Cr_2O_3-KCl, Fe_2O_3-KCl, Cr_2O_3-KOH, Fe_2O_3-KOH systems

In Publication V, the reactions of KOH(s,l) and KCl(s,l) with the protective oxide components formed on FeCr-alloys were studied. The detected reaction product, K_2CrO_4(s), was the same when KOH(s,l) or KCl(s,l) reacted with Cr_2O_3(s). KOH(s,l) seemed to be much more reactive than KCl(s,l), but the reactions seemed similar, as shown in Figures 18 and 19. There were no signs of any chlorine-containing reaction products when KCl(s,l) was used as the reactant, either with Cr_2O_3(s) or Fe_2O_3(s). In fact, with Fe_2O_3(s), we could not identify any reaction with KCl(s,l) in the studied temperature range (25-800 °C). These results provide convincing evidence that the K_2CrO_4 formation plays a major role in the initial breakdown of the protective oxides with both salts. It was also found that once the K_2CrO_4(s,l) has formed, it can react further with Cr_2O_3(s) at temperatures higher than 400 °C and form $K_2Cr_2O_7$(s,l). This is a very interesting observations, as it can explain the so-called memory effect in the KCl-induced corrosion studies (corrosion continues even after KCl is removed from the environment). The similarities of the reaction products in KOH(s,l)- or KCl(s,l)-induced corrosion reactions suggest that perhaps the initial reactions are actually identical. It is known that KCl(s,l,g) is much more stable thermodynamically than KOH(s,l,g). However, in a water-containing environment, KCl(s,l,g) is in equilibrium with KOH(s,l,g). Depending on the temperature and partial pressure of water in the system, there is always a small amount of KOH(s,l,g) and HCl(g) formed from KCl(s,l,g), as shown in Figure 20. Therefore, it is suggested that K_2CrO_4 formation starts by the decomposition of KCl(s,l,g) to KOH(s,l,g) and HCl(g) and the subsequent reaction of KOH(s,l,g) with Cr_2O_3(s). The reaction rate of the KCl(s,l,g) reaction with Cr_2O_3(s) is much lower than KOH(s,l,g) reacting with it, because the limiting factor is the decomposition of KCl(s,l,g) to KOH(s,l,g) and HCl(g). This explanation would unify the initial corrosion mechanisms for both salts. However, the validity of the hypothesis requires further experimental investigations.

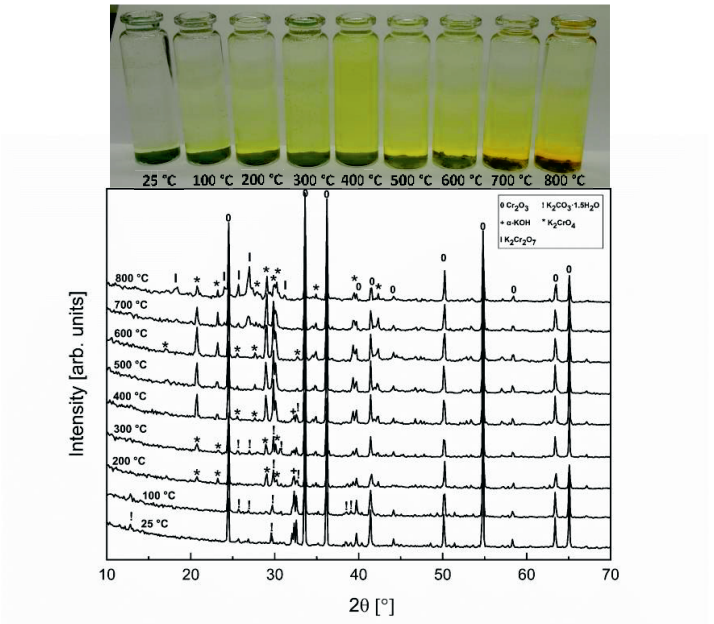

Figure 18. XRD analysis of KOH-Cr_2O_3 mixture after furnace exposures. The photograph on the top shows the characteristic yellow and orange colours of the CrO_4^{2-} and $Cr_2O_7^{2-}$ ions when the reaction product dissolved in water. From Publication V, licensed under a Creative Commons Attribution 3.0 Unported Licence.

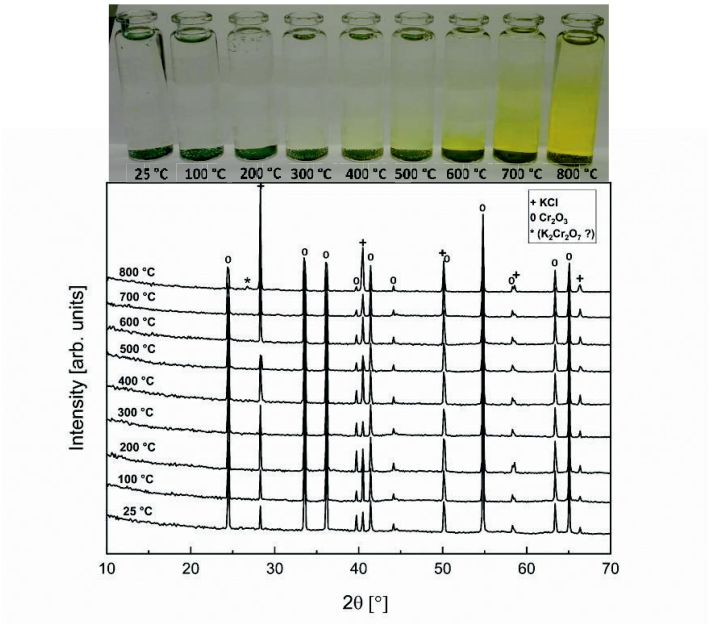

Figure 19. XRD analysis of KCl-Cr_2O_3 mixture after furnace exposures. The photograph on top shows the characteristic yellow colour of the CrO_4^{2-} ions when the reaction product dissolved in water. From Publication V, licensed under a Creative Commons Attribution 3.0 Unported Licence.

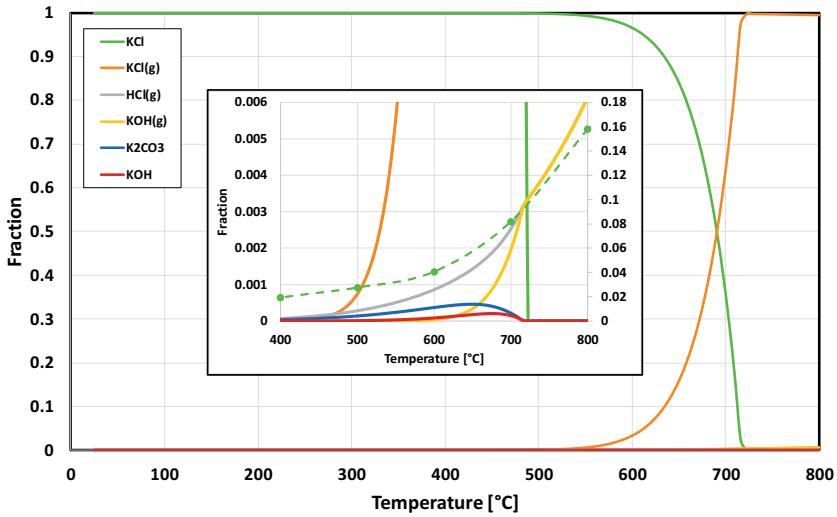

Figure 20. Thermodynamic stability of KCl in humid air, calculated with HSC v6.12 software. The inset is a zoomed image from the bottom-right corner of the chart. The green dashed line in the inset (right y-axis) shows the trend of the experimentally determined amount of potassium reacted to K_2CrO_4 when KCl and Cr_2O_3 reacted in the furnace. The fraction of reacted potassium is approximately 25 times higher than predicted by thermodynamics. This can be explained by Le Châtelier's principle, as the reactive product in the decomposition reaction (KOH) is continuously consumed in the reaction with Cr_2O_3. From Publication V, licensed under a Creative Commons Attribution 3.0 Unported Licence.

8. Conclusions

Fouling and corrosion in biomass-fired boilers continue to be the most important obstacles that prevent the use of a steam parameter as high as that in coal-fired units. The research in this thesis was concentrated on the effect of potassium hydroxide in fouling and corrosion processes. Prior to this work, there were no systematic studies available on the effects of potassium hydroxide on fireside corrosion and fouling in boilers. Several interesting observations were made, and a physicochemical mechanism was developed that could explain these observations. The physicochemical model is linked to the amount of the deposit-forming elements in the fuel: the excess of potassium compared to the amounts of sulphur and chlorine on molar basis predicts the formation of KOH(g)/K_2CO_3(g) in the flue gases. The nucleation phenomena of K_2CO_3(g) to K_2CO_3(s) aerosol particles plays a key role in evaluating the rationale of the 2KOH(g) → 2KOH(s,l) + CO_2(g) → K_2CO_3(s) + H_2O(g) mechanism in K_2CO_3(s) formation on the heat transfer surfaces. The nucleation rate is always kinetically controlled, and therefore, it is very difficult to estimate the actual K_2CO_3(s) aerosol formation rate versus the KOH(g) => KOH(s,l) condensation rate theoretically. Furthermore, because K_2CO_3(g) is not very stable thermodynamically in the gas phase, there is doubt that the high supersaturation ratios required for homogenous nucleation can be reached for K_2CO_3(g) → K_2CO_3(s) nucleation in real boilers. Recent experimental results

suggest that homogeneous $K_2CO_3(g) \rightarrow K_2CO_3(s)$ nucleation can happen in the gas phase in conditions relevant to post-combustion flue gases in boilers (Weng, et al., 2018), but are the kinetics of this process so fast that it captures all the KOH(g) diffusing towards the tube surface in the boundary layer surrounding the tube? The boundary layer thickness was estimated to be $\approx$ 1 mm, and the diffusion time of KOH(g) across that boundary layer to be in the order of 1.5-5.2 ms in Publication II. Also, in Publication IV, it was shown effectively that even if the $K_2CO_3(g) \rightarrow K_2CO_3(s)$ nucleation is assumed to be infinitively fast, there is still some KOH(g) left in the boundary layer at temperatures 400–600 °C, because of the unfavourable thermodynamics of $K_2CO_3(g)$ formation, as shown in Figure 17. After all, aerosol formation by homogeneous nucleation requires the gas phase $K_2CO_3(g)$ to form first and then nucleate to the corresponding solid $K_2CO_3(s)$.

However, if the flue gas contains a large number of other particles present in the boundary layer of the heat exchanger surface ($K_2SO_4(s)$ aerosols, Al-silicates and other ash particles), then the combined surface area of these particles may be so large that the KOH(g), in heterogeneously reacting on these particles to $K_2CO_3(s)$, and the KOH(g), is consumed before reaching the tube surface. This heterogeneous mechanism furthermore enables the capture of KOH(g) at higher gas temperatures, because now the relevant equilibrium is the KOH(g)-$K_2CO_3(s)$, which leads to the capture of any KOH(g) at surface temperatures lower than $\approx$ 700 $^\circ$ C, as shown in Figure 7a. Because of the short residence times of the reactants in the boundary layer for the reaction to happen and the substantial difficulties in taking into account all the reaction kinetic and mass transfer effects involved, this author is unaware how to model the situation properly with theoretical methods. Additionally, the experimental evidence to prove or disprove the existence of KOH(g) in the gas phase and KOH(s,l) in the deposits was indirect, because of the experimental difficulties in identifying and quantifying KOH(s,l,g) in the flue gases or on the heat exchanger surfaces in real boilers. The recently developed optical measurement techniques for detecting KOH(g) in the gas phase hold promise to be able to measure its partial pressures in industrial-scale combustors, provided that the techniques can be adapted for industrial environments. The direct detection of condensing KOH(s,l) on the heat transfer surfaces remains an unresolved problem, and future studies concerning its effects will probably still rely on indirect correlations and arguments.

8.1 Difficulties in detecting KOH(s,l,g) in-situ

The results obtained gained in this thesis concerning the effect of KOH(s.l,g) in fouling and corrosion are indirect. There are no direct measurements of the existence of KOH(s,l,g) in the flue gases or on heat transfer surfaces. This is true for the rest of the scientific literature, too. Only very few papers claim direct evidence of KOH(g) in the flue gases or KOH(s,l) in the deposits. This can be attributed to the reactivity of KOH(s,l,g). Recently, some papers have reported new measurement techniques that can quantify the gas-phase potassium speciation (K(g), KCl(g), KOH(g)) in the flue gases (Sorvajärvi, DeMartini, Rossi, Toivonen, & Juha, 2014; Weng, et al., 2019). If these techniques can be adapted to large-scale industrial combustors, they provide hope of resolving the partial pressure distributions of gaseous potassium species as a function of location in the boiler. This type of measurement would provide valuable information for the boiler manufactures and corrosion engineers.

Condensed phase KOH(s,l) is even more difficult to detect than KOH(g). Detailed laboratory work has shown that even when trying to produce condensed alkali hydroxides on a probe surface using alkali-doped hydrogen flame, the result was an alkali carbonate deposition product after probe cool-down that was detected directly with Raman spectroscopy. The alkali hydroxide was detected only indirectly by measuring the pH of the water solution where the deposit was dissolved. This showed a value of 14, which is too high for pure alkali carbonate, and therefore it was concluded that the deposit was a mixture of alkali hydroxide and carbonate (Steinberg & Schofield, 2002). It seems that the CO_2(g) concentration in the ambient air is enough to transform the condensed hydroxide to carbonate during deposition and the probe cool-down period. There is one paper that claims the existence of KOH(s) in deposits from large-scale boilers. However, the identification was done by XRD, and α-KOH(s) has only two intensive XRD peaks (002 and 110 at 32.173° and 32.412°) in the typical powder XRD 2θ range (10-70°). Because the deposit sample contained many other compounds, too, the number of peaks was large, and there may have been other compounds that were causing the XRD peaks (Wu, Bashir, Jensen, Sander, & Glarborg, 2013).

The condensed KOH(s) can also be amorphous, which would prevent its detection by XRD analysis. Furthermore, KOH(s) is known to be highly deliquescent, which can lead to the transformation of the crystalline α-KOH(s) to a KOH-water solution if exposed to ambient air for a prolonged period. All these properties of KOH(s,l) make it a difficult compound to be identified unambiguously in the deposits. However, that does not mean that it cannot take part in the deposit formation and corrosion reactions. In the future, the combination of on-line electrochemical techniques could provide proof of condensing KOH(l) if the signal fingerprints could be somehow correlated with the condensate chemistry.

8.2 Evolution of molar balances of K, Na, S and Cl during the growth and geological transformation of biomass

Categorizing the fuels with equation (13) results in an extremely clear distinction between biomass-based fuels and fossil fuel, as shown below in Table 4. Furthermore, the fuels seem to arrange in ascending order with the geological age of the fuel. This is an interesting observation and may indicate some general mechanism, first, in the uptake of K, S and Cl to the biomass during its growth: the faster the plant part grows, the higher the free potassium content (not associated with sulphate or chloride anions). Indeed, the suppression of plant growth by chloride and sulphate has been reported in the literature (Reich, et al., 2017; Eaton, 1942). Furthermore, it has been suggested that K^+-ion transport in the plant cells plays a role in the CO_2(g) absorption mechanism, functioning as a counter ion for the HCO_3^- ions formed in the chloroplast during the CO_2(g) absorption (Hauser, Eichelmann, Oja, Heber, & Laisk, 1995). This could explain the higher free potassium content in the palisade cells (green parts where the photosynthesis takes place), compared to the cells forming the stem and roots of the plant.

On the other hand, the changes in the concentrations of these elements in the biomass during its transformation to fossil fuel also seems to have a common mechanism that keeps lowering the potassium content and increasing the sulphur content of the fossil fuel as a function of its geological age. The generality of these observations and mechanisms involved would be an interesting research topic for future studies.

Table 4. Different fuels sorted with free potassium content.

Fuel	KOH(g) [mmol/kg]	Geological age
Brasica Carinata straw	202.8	Young biomass
Wheat straw	157.6	
Maize straw	77	
Wheat Marius straw	72.2	
Rape straw	47.4	
Forest residue	27	
Bark (pine)	9	Old biomass
Sawdust (pine)	7.9	
Peat, surface	−33.2	Young fossil fuels
Peat, carex	−106.7	
Rhein brown coal	−177.4	Middle aged fossil fuels
Iowan Rawhide coal	−248.2	
Polish bituminous coal	−401.8	Old fossil fuels
Columbian bituminous coal	−541.3	
Illinois no 6, bituminous coal	-1687.5	

8.3 Suggestions for further studies

In the corrosion literature, the breakdown of the protective Cr_2O_3 layer in biomass-fired boilers has been explained with the overall chemical reaction:

$$4KCl + Cr_2O_3 + 1½\ O_2(g) + 2H_2O(g) \Leftrightarrow 2K_2CrO_4 + 4HCl(g) \quad (R39)$$

Based on the results of this study, it is proposed that this reaction proceeds in two steps:

$$4KCl + 4H_2O(g) \Leftrightarrow 4KOH + 4HCl(g) \quad (R40)$$

$$4KOH + Cr_2O_3 + 1½\ O_2(g) \Leftrightarrow 2K_2CrO_4 + 2H_2O(g) \quad (R41)$$

There should be differences in the evolution profile of HCl(g) relative to the formation K_2CrO_4 as a function of time with different mechanisms (Lehmusto, et al., 2019). If KCl reacts directly with Cr_2O_3, the formation of K_2CrO_4 and the evolution of HCl(g) should be simultaneous. If the mechanism follows reactions R40 and R41, there should be a time gap between HCl(g) evolution and K_2CrO_4 formation. Therefore, one could organize an experimental setup where a preheated Cr_2O_3 sample is suddenly exposed to KCl, and then the K_2CrO_4 formation and HCl(g) evolution would be measured simultaneously. K_2CrO_4 formation could be detected optically, and HCl(g) formation could be detected with an HCl(g) sensor or with a mass spectroscopic method, for example. From the K_2CrO_4 and HCl(g) formation profiles, one could obtain greater insight into the kinetics and mechanisms of the reaction.

9. References

Aho, M., & Silvennoinen, J. (2004). Preventing chlorine deposition on heat transfer surfaces with aluminium-silicon rich biomass residue and additive. *Fuel, 83*, 1299-1305.

Anicic, B., Lin, W., Kim, D.-J., & Wu, H. (2018). Agglomeration mechanism in biomass fluidized bed combustion- Reaction between potassium carbonate and silica sand. *Fuel Processing Technology, 173*, 182-190.

Antolini, E. (2011). The stability of molten carbonate fuel cell electrodes: A review of recent improvements. *Applied Energy, 88*, 4274-4293.

Aref´´ev, K., Ivashchenko, N., Suslova, L., & Khomchenkov, B. (1969). The settling out of ionizing additives from a stream of combustion products. *Journal of Engineering Physics and Thermophysics, 16*, 731-734.

Backman, R., Enestam, S., & Zevenhoven, R. (1998). *Structure and Behaviour of Inorganics in Recovery Boilers - A Modelling Approach.* Åbo: Liekki 2 Technical Review Åbo Akademi University.

Backman, R., Hupa, M., & Uppstu, E. (1987). Fouling and corrosion mechanisms in the recovery boiler superheater area. *Tappi Journal, 70*, 123-127.

Bankiewicz, D., Enestam, S., Yrjas, P., & Hupa, M. (2013). Experimental studies of Zn and Pb induced high temperature corrosion of two commercial boiler steels. *Fuel Processing Technology, 105*, 89-97.

Bankiewicz, D., Yrjas, P., & Hupa, M. (2009). High temperature corrosion of steam tube materials exposed to zinc salts. *Energy and Fuels, 23*, 3469-3474.

Blomberg, T. (2007). Free alkali-index for optimizing the fuel mixture in biomass co-firing. *ECI conference proceedings, Heat exhanger fouling VII.* Tomar.

Blomberg, T., Hiltunen, M., & Makkonen, P. (2001). Modern CFB Concept for Combustion of Recovered Fuel: Design for Improved Availability. *16th International Conference on Fluidized Bed Combustion.* Reno.

Boström, D., Skoglund, N., Grimm, A., Boman, C., Öhman, M., Broström, M., & Backman, R. (2012). Ash Transformation Chemistry during Combustion of Biomass. *Energy and Fuels, 26*, 85-93.

Bozzini, B., Barella, S., Bogani, F., Giovannelli, G., Natali, S., Scarselli, G., & Boniardi, M. (2012). Corrosion of stainless steel grades in molten NaOH/KOH eutectic at 250 °C: AISI304 austenitic and 2205 duplex. *Materials and Corrosion , 63*, 967-978.

Broström, M., Enestam, S., Backman, R., & Mäkelä, K. (2013). Condensation in the KCl-NaCl system. *Fuel Processing Technology, 105*, 142-148.

Budkuley, J. S., & Patil, K. (1990). Synthesis, infrared spectra and thermoanalytical properties of transition metal sulfite hydrazine hydrates. *Journal of Thermal Analysis, 36*, 2583-2592.

Cabrera, N., & Mott, N. (1949). Theory of the oxidation of metals. *Reports on Progress in Physics, 12*, 163-184.

Cantatore, V., Ogaz, M. A., Liske, j., Jonsson, T., Svensson, J.-E., Johansson, L.-G., & Panas, I. (2019). Oxidation Driven Permeatation of Iron Oxide Scales by Chloride from Experiment Guided First-Principles Modelling. *Journal of Physical Chemistry C, 123*, 25957-25966.

Channiwala, S.A., Parikh, & P.P. (2002). A unified correlation for estimating HHV of solid, liquid and gaseous fuels. *Fuel, 81*, 1051-1063.

Chen, C., Luo, Z., Yu, C., Wang, T., & Zhang, H. (2017). Transformation behavior of potassium during pyrolysis of biomass. *RSC Advances, 7*, 31319-31326.

CRC Handbook of Chemistry and Physics. (2004). CRC Press.

D.E., R., & Nagarajan, R. (1987). Vapor Deposition and Condensate Flow on Combustion Turbine Blades: Theoretical Model to Predict/Understand Some Corrosion Rate Consequences of Molten Alkali Sulfate Deposition in the Field of Laboratory. *International Journal of Turbo & Jet-Engines, 4*, 323-347.

Damoe, A. J., Jensen, P. A., Frandsen, F. J., Wu, H., & Glarborg, P. (2017). Fly Ash Formation during Suspension Firing of Biomass: Effects of Residence Time and Fuel Type. *Energy and Fuels, 31*, 555-570.

Davidsson, K. O., Åmand, L.-E., & Leckner, B. (2007). Potassium, Chlorine, and Sulfur in Ash, Particles, Deposits, and Corrosion during Wood Combustion in a Circulating Fluidized-Bed Boiler. *Energy and Fuels, 21*, 71-81.

Dayton, C., D., French, R. J., & MIlne, T. A. (1995). Direct obseravtion of Alkali Vapor Release during Biomass Combustion and Gasification. 1. Application of Molecular Beam/Mass Spectrometry to Switchgrass Combustion. *Energy and Fuels, 9*, 855-865.

Dayton, D. C., Frederick, & J. W. (1996). Direct observation of alkali vapor release during biomass combustion and gasification. 2. Black liquor combustion at 1100 C. *Energy and Fuels, 20*, 284-292.

Demirbas, & Ayhan. (1997). Calculation of higher heating values of biomass fuels. *Fuel, 76*, 431-434.

Eaton, F. M. (1942). Toxicity and accumulation of chloride and sulfate salts in plants. *Journal of Agricultural Research, 64*, 357-399.

Ellingham, H. (1944). Reducibility of oxides and sulphides in metallurgical processes. *Journal of the Society of Chemical Industry, 63*, 125.

Frandsen, F., van Lith, S. C., Korbee, R., Yrjas, P., Backman, R., Obernberger, I., . . . Jöller, M. (2007). Quantification of the release of inorganic elements from biofuels. *Fuel Processing Technology, 88*, 1118-1128.

Geelhoed, P., Westerweel, J., Kjelstrup, S., & Bedeaux, D. (2008). Thermophoresis. In *Encyclopedia of Microfluidics and Nanofluidics* (pp. 2061-2064). Boston: Springer.

Giddey, S., Badwal, S., Kulkarni, A., & Munnings, C. (2012). A comprehensive review of direct carbon fuel cell technology. *Progress in Energy and Combustion Science, 38*, 360-399.

Grabke, H., Reese, E., & Spiegel, M. (1995). The effects of chlorides, hydrogen chloride, and sulfur oxide in the oxidation of steels below deposits. *Corrosion Science, 37*, 1023-1043.

Gruber, T., Schulze, K., Scharler, R., & Obernberger, I. (2015). Investigation of the corrosion behaviour of 13CrMo4-5 for biomass fired boilers with coupled onlne corrosion and deposit probe measurements. *Fuel, 144*, 15-24.

Guo, L., Calo, J. M., DiCocco, E., & Bain, E. J. (2013). Development of a Low Temperature , Molten Hydroxide Direct Carbon Fuel Cell. *Energy and Fuels, 27*, 1712-1719.

Hansen, S. B., Jensen, P. A., Frandsen, F. J., Sander, B., & Glarborg, P. (2017). Mechanistic Model for ASh Deposit Formation in Biomass Suspension Firing. Part 1: Model Verification by Use of Entrained Flow Reactor Experiments. *Energy and Fuels, 31*, 2771-2789.

Harb, J., & Smith, E. (1990). Fireside corrosion in pc-fired boilers. *Progress in Energy and Combustion Science, 16*, 169-190.

Hauser, M., Eichelmann, H., Oja, V., Heber, U., & Laisk, A. (1995). Stimulation by Light of Rapid pH Regulation in the Chloroplast Stroma in Vivo as

Indicated by CO2 Solubilization in Leaves. *Plant Physiology, 108*, 1059-1066.
Henderson, P., Szakálos, P., Pettersson, R., C., A., & Högberg, J. (2006). Reducing superheater corrosion in wood-fired boilers. *Materials and Corrosion, 57*, 128-134.
Hendry, A. (1980). Corrosion of austenitic steels in molten sulphate deposits. *Corrosion Science, 20*, 383-404.
Herzog, T., Müeller, W., Spiegel, W., . . . Schneider, D. (2012). Corrosion caused by Dew Point and Deliquescent Salts in the Boiler and Flue Gas Cleanings. In *Thomé-kozmiensky, K.J and Thiel, S., Waste Management, Volume 3* (Vol. 3, pp. 343-358). Neuruppin: TK Verlag.
Hesketh; J.A.;Walker; P.J. (2005). Effects of wetness in steam turbines. *Proceedings of the Institution of Mechanical Engineers, Part C: Journal of Mechanical Engineering Science, 219*, 1301-1314.
Honghi, T., Mao, X., & Chartrand, P. (2009). Effects of sulphide on melting temperature of smelt and carryover in kraft recovery boilers. *TAPPI EPE Conference.* Memphis.
Hsu, H. S., DeVan, J. H., & Howell, M. (1987). Solubilities of LiFeO2 and (Li,K)K2CrO4 in Molten Alkali Carbonates at 650 °C. *Journal of the Electrochemical Society, 134*, 2146-2150.
Hultgren, N., & Brewer, L. (1956). Gaseous molybdenum oxychloride. *Journal of Physical Chemistry, 60*, 947-949.
Hupa, M. (2005). Interaction of fuels in co-firing in FBC. *Fuel, 84*, 1312-1319.
Hupa, M. (2012). Ash-Related Issues in Fluidized-Bed Combustion of Biomasses: Recent Research Highlights. *Energy and Fuels, 26*, 4-14.
Hupa, M., Karlström, O., & Vainio, E. (2017). Biomass combustion technology development - It is all about chemical details. *Proceedings of the Combustion Institute, 36*, 113-134.
IEA. (2017). *CO2 emissions from Fuel Combustion 2017.* IEA.
Ishitsuka, T., & Nose, K. (2000). Solubility study on protective oxide films in molten chlorides created by refuse incineration environment. *Materials and Corrosion, 51*, 177-181.
Jeng, J., Zou, T.S., Wu, J., Jiang, C., . . . D.Y. (2009). Study on Combustion Characteristics of Lignite in a CFB boiler. *Proceedings of the 20th International Conference on Fluidized Bed Combustion.* Xi'an.
Jiménez, S., & Ballester, J. (2004). Formation and Emission of Submicron Particles in Pulverized Olive Residue (Orujillo) Combustion. *Aerosol Science and Technology, 38*, 707-723.
Jiménez, S., & Ballester, J. (2005). A Comparastive Study of Different Methods for the Sampling of High Temperature Combustion Aerosols. *Aerosol Science and Technology, 39*, 811-821.
Jiménez, S., & Ballester, J. (2005). Influence of operating conditions and role of sulfur in the formation of aerosols from biomass combustion. *Combustion and Flame, 140*, 346-358.
Jiménez, S., & Ballester, J. (2007). Formation of alkali sulphate aerosols in biomass combustion. *Fuel, 86*, 486-493.
Karampinis, E., Grammelis, P., Agraniotis, M., Violidakis, I., & Kakaras, E. (2014). Co-Firing of biomasss with coal in thermal power plants: technology schemes, impacts, and future perspectives. *WIREs Energy and Environment, 3*, 384-399.
Karlsson, S., Pettersson, J., Johansson, L.-G., & Svensson, J.-E. (2012). Alkali induced High Temperature Corrosion of Stainless Steel: The Influence of

NaCl, KCl and CaCl2. *Oxidation of Metals, 78*, 83-102.
Koukkari, P. (2014). *Introduction to constrained Gibbs energy methods in process and materials research, VTT Technology 160.* Espoo: VTT.
Laxminarayan, Y., Nair, A. B., Jensen, P. A., Wu, H., Frandsen, F. J., Sander, B., & Glarborg, P. (2018). Tensile Adhesion Strength of Biomass Ash Deposits: Effect of the Temperature Gradient and Ash Chemistry. *Energy and Fuels, 32*, 4432-4441.
Lee, K. N., & Shores, D. A. (1990). Transport considerations in the Hot Corrosion of Ni by Molten Alkali Carbonates. *Journal of the Electrochemical Society, 137*, 859-871.
Lehmusto, J., Linddberg, D., Yrjas, P., Skrifvars, B.-J., & Hupa, M. (2012). Thermogravimetric studies of high temperature reactions between potassium salts and chromium . *Corrosion Science, 59*, 55-62.
Lehmusto, J., Olin, M., Viljanen, J., Kalliokoski, J., Mylläri, F., Toivonen, J., . . . Hupa, L. (2019). Detection of gaseous species during KCl-induced high-temperature corrosion by the means of CPFAAS and CI-APi-TOF. *Materials and Corrosion, early view*.
Lind, T., Kauppinen, E. I., Hokkinen, J., Jokiniemi, J. K., Orjala, M., Aurela, M., & Hillamo, R. (2006). Effect of Chlorine and Sulfur on Fine Particle Formation in Pilot-Scale CFBC of Biomass. *Energy and Fuels, 20*, 61-68.
Lindberg, D., Backman, R., & Chartrand, P. (2007). Thermodynamic evaluation and optimization of the (Na2CO3+Na2SO4+NaS2+K2CO3+K2SO4+K2S) system. *Journal of Chemical Thermodynamics, 39*, 942-960.
Liu, W., Zhang, Z., Xie, X., Yu, Z., von Gadow, K., Xu, J., . . . Yang, Y. (2017). Analysis if the Global Warming Potential of Biogenic CO2 Emission in Life Cycle Assesments. *Scientific Reports, 7*, 39857.
Ma, W., Terrence, W., Frandsen, F. J., Beibei, Y., & Guanyi, C. (2020). The fate of chlorine during MSW incineration: Vaporization, transformation, deposition, corrosion and remedies. *Progress in Energy and Combustion Science, 76*, 100789.
Mahanen, J., Vänskä, K., & Zabetta, E. C. (2015). Corrosion monitoring in commercial CFBs. *22nd international conference on fluidized bed conversion.* Turku.
Mason, P. E., Darvell, L. I., Jones, J. M., & Williams, A. (2016). Observation on the release of gas-phase potassium during the combustion of single particles of biomass. *Fuel, 182*, 110-117.
Mason, P. E., Jones, J. M., Darvell, L., & Williams, A. (2017). Gas phase potassium release from a single particle of biomass during high temperature combustion. *Proceedings of the Combustion Institute, 36*, 2207-2215.
Montgomery, M., Carlsen, B., Biede, O., & Larsen, O. (2002). Superheater corrosion in biomass-fired power plants: Investigation of welds. *Corrosion, 02379*, 1-20.
Montgomery, M., Karlsson, A., & Larsen, O. (2002). Field test corrosion experiments in Denmark with biomass fuels Part 1: Straw-firing. *Corrosion 2002*, *53*, pp. 121-131. Denver.
Mortensen, R. M., Hashemi, H., Wu, H., & Glarborg, P. (2019). Modeling post-flame sulfation of KCl and KOH in bio-dust combustion with full and simplified mechanisms. *Fuel, 258*, 116147.
Mrowec, S., & Przybylski, K. (1985). Transport properties of sulfide scales and sulfidation of metals and alloys. *Oxidation of Metals, 23*, 107-139.

Mueller, C., Skrifvars, B.-J., Backman, R., & Hupa, M. (2007). Ash deposition prediction in biomass fired fuidized bed boilers - combination of CFD and advanced fuel analysis. *Progress in Computational Fluid Dynamics, 3*, 112-120.

Neuenschwander, P., & Good J, N. T. (1998). Combustion efficiency in biomass furnaces with flue gas condensation . *Biomass for Energy and Industry, 10th European Conference and Technology Exhibition* . Würzburg.

Nickel Institute. (1973). *Corrosion Resistance of Nickel and Nickel-Containing Alloys in Caustic Soda and Other Alkalies, Publication No 281.* Nickel Development Institute.

Nielsen, H., Baxter, L., Sclippab, G., Morey, C., Frandsen, F., & Dam-Johansen, K. (2000). Deposition of potassium salts on heat transfer surfaces in straw-fired boilers: a pilot-scale study. *Fue, 79*, 131-139.

Nielsen, H., Frandsen, F., Dam-Johansen, K., & Baxter, L. (2000). The implications of chlorine-associated corrosion on the operation of biomass-fired boilers. *Progress in Energy and Combustion Science, 26*, 283-298.

Niu, Yanqing, Tan, H., & Hui, S. (2016). Ash-related issues during biomass combustion: Alkali-induced slagging, silicate melt-induced slagging (ash fusion), agglomeration, corrosion, ash utilization, end related countermeasures. *Progress in Energy and Combustion Science, 52*, 1-61.

Nutalapati, D., Gupta, R., Moghtaderi, B., & Wall, T. (2007). Assessing slagging and fouling during biomass combustion: A thermodynamic approach allowing for alkali/ash reactions. *Fuel Processing Technology, 88*, 1044-1052.

Ota, K.-i., Takeishi, Y., Shibata, S., Yohitake, H., Kamiya, N., & Yamazaki, N. (1995). Solubility of Cobalt Oxide in Molten Carbonate. *Journal of the Electrocemical Society, 142*, 3322-3326.

Otsuka, N. (2008). A thermodynamic approach on vapor-condensation of corrosive salts from flue gas on boiler tubes in waste incinerators. *Corrosion Science, 50*, 1627-1636.

Pettersson, J., Folkeson, N., Johansson, L.-G., & Svensson, J.-E. (2011). The Effects of KCl, K2SO4 and K2CO3 on the High Temperature Corrosion of a 304-Type Austenitic Stainless Steel. *Oxidation of Metals, 76*, 93-109.

Rapp, R. (2002). Hot corrosion of materials: a fluxing mechanism? *Corrosion Science, 44*, 209-221.

Rapp, R. A., & Otsuka, N. (2009). The Role of Chromium in the Hot Corrosion of Metals. *ECS Transactions, 16*, 271-282.

Reich, M., Aghajanzadeh, T., Helm, J., Parmar, S., Hawkesford, M. J., & De Kok, L. J. (2017). Chloride and sulfate salinity differently affect biomass mineral nutrient composition and expression of sulfate trnasport and assimilation genes in Brassica rapa. *Plant Soil, 411*, 319-332.

Retschitzegger, S., Brunner, T., Obernberger, I., & Waldmann, B. (2013). Assessment of Online Corrosion Measurements in Combination with Fuel Analyses and Aerosol and Deposit Measurements in a Biomass Combined Heat and Power Plant. *Energy and Fuels, 27*, 5670-5683.

Retschitzegger, S., Gruber, T., Brunner, T., & Obernberger, I. (2015). Short term online corrosion measurements in biomass fired boilers. Part 1: Application of a newly developed mass loss probe. *Fuel Processing Technology, 137*, 148-156.

Roine. (2014). *HSC Chemistry chemical equilibrium software.* Pori: Outotec Oy.

Rosner, Daniel, & Liang, B. (1988). Experimental studies of deposition rates in the presence of alkali sulfate vapor scavenging by submicron particles in

combustion boundary layers. *Chemical Engineering Communications, 64*, 27-46.
Salib, K. A., El-Maraghy, S. B., El-Wafa, S. M., & El-Sayed, S. M. (1989). Normal sulphites of metals. *Transition Metal Chemistry, 14*, 306-308.
Santoianni, Dawn. (2015). Setting the Benchmark: The World's Most Efficient Coal-Fired Power Plants . *Cornerstone, 3*(1).
Schofield, K. (2003). A new Method to Minimize High-Temperature Corrosion Resulting from Alkali Sulfate and Chloride Deposition in Combustion Systems. I. Tungsten Salts. *Energy and Fuels, 17*, 191-203.
Sengelov, W. L., Hansen, T. B., Bartolome, Carmen, Wu, H., Pedersen, K. H., . . . Glarborg, P. (2013). Sulfation of Condensed Potassium Chloride ny SO2. *Energy and Fuels, 27*, 3283-3289.
Shi, L., Zhang, Y., & Shih, S. (1992). The Effect of K2SO4 Additive in Na2SO4 Deposits on Low Temperature Hot Corrosion of Iron-Aluminium Alloys . *Oxidation of Metals, 38*, 385-405.
Singh, H., Puri, D., & Prakash, S. (2007). An overview of Na2SO4 and/or V2O5 induced hot corrosion of Fe- and Ni-based superalloys. *Reviews on Advanced Materials Science , 16*, 27-50.
Smith, G. (1956). *Corrosion of materials in fused hydroxides.* Oak Ridge: Oak Ridge Nationl Laboratory.
Sorvajärvi, T., DeMartini, N., Rossi, J., Toivonen, & Juha. (2014). In Situ Measurement Technique for Simultaneous Detection of K, KCl, and KOH Vapors Released during Combustion of Solid Biomass Fuel in a Single Particle Reactor. *Applied Spectroscopy, 68*, 179-184.
Steinberg, M., & Schofield, K. (2002). The Controlling Chemistry of Surface Deposition from Sodium and Potassium Seeded Flames Free of Sulfur or Chlorine Impurities. *Combustion and Flame, 129*, 453-470.
Stringer, J. (1977). Hot corrosion of high-temperature alloys. *Annual Review of Materials Science, 7*, 477-509.
Stringer, J., & Wright, I. G. (1995). Current Limitations of High-Temperature Alloys in Practical Applications. *Oxidtion of Metals, 44*, 265-308.
Tran, H., Gonsko, M., & Mao, X. (1999). Effect of composition on the first melting temperature of fireside deposits in recovery boilers. *Tappi Journal, 82*, 93-100.
Tran, H., Mao, X., & Barham, D. (1992). Recovery boiler air port corrosion - Part 1: The stability of NaOH and KOH in the presence of CO2. *Tappi Engineering Conference.* Boston.
Tsai, S., Huntz, A., & Dolin, C. (1996). Growth mechanism of Cr2O3 scales: oxygen and chromium difusion, oxidation kinetics and effect of yttrium. *Materials Science and Engineering A, A212*, 6-13.
Tuurna, S. (2011). *HIgh performance materials and corrosion control for efficient and low emission biomass and waste combustion (HICOR) - final report.* Tampere: VTT.
Tzvetkoff, T., & Gencheva, P. (2003). Mechanism of formation of corrosion layers on nickel and nickle-based alloys in melts containing oxyanions-a review. *Materials Chemistry and Physics, 82*, 897-904.
Tzvetkoff, T., & Girginov, A. (1995). Corrosion of nickel, iron, cobalt and their alloys in molten salt electrolytes. *Journal of Materials Science, 30*, 5561-5575.
van den Broek, R., FaaiJ, A., & van Wijk, A. (1996). Biomass combustion for power generation. *Biomass and Bioenergy, 11*, 271-281.
Vossen, J., Plomp, L., de Wit, J., & Rietveld, G. (1995). Corrosion behavior of

Stainless Steel and Nickel-Base Alloys in Molten Carbonate. *Journal of Electrochemical Society, 142*, 3327-3335.

Wang, G., Jensen, P. A., Wu, H., Frandsen, F. J., Sander, B., & Glarborg, P. (2018). Potassium Capture by Kaolin, Part 2: K2CO3, KCl and K2SO4. *Energy and Fuels, 32*, 3566-3578.

Wang, G., Jensen, P. A., Wu, H., Frandsen, F. J., Sander, B., & Glarborg, P. (2018). Potassium Capture by Kaoling, Part 1: KOH. *Energy and Fuels, 32*, 1851-1862.

Wei, X., Schnell, U., & Hein, K. R. (2005). Behaviour of gaseous chlorine and alkali metals during biomass thermal utilization. *Fuel, 84*, 841-848.

Weng, W., Brackmann, Christian, Leffler, T., Aldén, M., & Li, Z. (2019). Ultraviolet Absorption Cross Sections of KOH and KCl for Nonintrusive Species-Specific Quantitative Detection in Hot Flue Gases . *Analytical Chemistry, 91*, 4729-4726.

Weng, W., Chen, Shuang, Wu, H., Glarborg, P., & Li, Z. (2018). Optical investigation of gas-phase KCl/KOH sulfation in post flame conditions. *Fuel, 224*, 461-468.

Werkelin, J., Skrifvars, B.-J., Zevenhoven, M., Holmblom, B., & Hupa, M. (2010). Chemical forms of ash-forming elements in woody biomass fuels. *Fue, 89*, 481-493.

Westberg, H. M., Byström, M., & Leckner, B. (2003). Distribution of Potassium, Chlorine, and Sulfur between Solid and Vapor Phases during Combustion of Wood Chips and Coal. *Energy and Fuels, 17*, 18-28.

Wiinikka, H., Rikard, G., Boman, C., Boström, D., & Öhman, M. (2007). Inluence of fuel ash composition on high temperature aerosol formation in fixed bed combustion of woody biomass pellets. *Fuel, 86*, 181-193.

Wu, H., Bashir, M. S., Jensen, P. A., Sander, B., & Glarborg, P. (2013). Impact of coal fly ash addition on ash transformation and deposition in a full-scale wood suspension-firing boiler. *Fuel, 113*, 632-643.

Young, D. (2016). *High Temperature Oxidation and Corrosion of Metals, 2nd edition.* Elsevier.

Young, D., & Pint, B. (2006). Chromium Volatilization Rates from Cr2O3 Scales into Flowing Gases Containing Water Vapor. *Oxidation of Metals, 66*, 137-153.

Zbogar, A., Frandsen, F., Jensen, P. A., & Glarborg, P. (2009). Shedding of ash deposits. *Progress in Energy and Combustion Science, 35*, 31-56.

Zhuang, D., & Edgar, J. (2005). Wet etching of GaN. AlN and SiC: A review. *Materials Science and Engineering R, 48*, 1-46.

This thesis deals with fouling and high temperature corrosion in furnaces and boilers using biomass based fuels as their energy source. The inorganic composition of biomass based fuels differs from coal and leads to increased fouling and corrosion rates in the combustors. This has forced the biomass fired combustors to operate at lower heat transfer surface temperatures, which leads to efficiency penalties compared to fossil fuel fired units. In addition, unscheduled maintenance breaks and corrosion of the construction materials increases the operation costs. Ash behaviour in the combustor, especially the behaviour of alkali metals, chlorine and sulphur has been identified as the key to understanding and mitigating fouling and corrosion issues in the combustors. Understanding the process chemistry of these elements in the combustors may lead to new methods of mitigating these issues and enable the biomass fired units to operate at higher conversion efficiencies. Potassium is the major alkali in biomass based fuels and substantial scientific work has already been done to understand its behaviour in the combustors. The earlier work has mostly concentrated on the fate of potassium chloride (KCl), because this compound is frequently found on heavily fouled and corroded heat transfer surfaces. This thesis is concentrated on the effect of potassium hydroxide (KOH) as a possible fouling/corrosion agent and as a possible precursor for KCl formation.

Aalto-DD 35/2020

ISBN 978-952-60-8982-9 (printed)
ISBN 978-952-60-8983-6 (pdf)
ISSN 1799-4934 (printed)
ISSN 1799-4942 (pdf)

Aalto University
School of Chemical Engineering
Department of Chemistry and Materials Science
www.aalto.fi

BUSINESS + ECONOMY

ART + DESIGN + ARCHITECTURE

SCIENCE + TECHNOLOGY

CROSSOVER

DOCTORAL DISSERTATIONS